Magnetic nanocarriers : From material design to magnetic manipulation

Clime, L.; Le Drogoff, B.; Zhao, S.; Zhang, Z.; Veres, T.

Publisher's version / Version de l'éditeur:
https://doi.org/10.1504/IJNT.2008.019839
International Journal of Nanotechnology, 5, 9-12, pp. 1268-1305, 2008-08

Magnetic nanocarriers: from material design to magnetic manipulation

L. Clime, B. Le Drogoff, S. Zhao, Z. Zhang and T. Veres*

Functional Nanomaterials
NRC, Industrial Materials Institute
75 Boul. de Mortagne, Boucherville, Canada J4B 6Y4
Fax: + 450 641-5105 E-mail: Teodor.Veres@cnrc-nrc.gc.ca
*Corresponding author

Abstract: Magnetic nanocarriers play an increasing role in various biomedical applications such as the separation of magnetically "tagged" DNA, drug delivery or identification of biological species. Recent developments in nanotechnology allow the fabrication of both artificial nanocarriers and magnetic separation devices which may achieve great performances at an incredibly small-volume sample handling. However, as the sizes of magnetic carriers and separation devices diminish, important theoretical and experimental challenges may occur mainly due to the important variations of the surface-to-volume ratio. Under these circumstances, intrinsic properties of individual carriers and their influence on functionality and performances of the magnetic manipulation have to be investigated with a higher degree of accuracy. In this paper, we present the state-of-the-art techniques for extracting accurate information about individual magnetic entities from magnetic measurements performed on ordered arrays or clusters of magnetic nano-objects of various dimensionalities and geometries. As the mutual magnetic interactions may be responsible for collective effects, both analytical and numerical techniques for evaluating the mutual interactions between magnetic nanoparticles and nanowires are reviewed, special emphasis being put on the dimensionality of their assemblages. As the efficiency of the manipulation and capture of individual magnetic carriers in magnetic confinement devices depend strongly on their size, the theoretical description of the motion of magnetic particles under various conditions of flow and field configurations become very important especially with the transition to the nanoscale regime. The equations of motion of magnetic nanocarriers in continuous-flow microfluidic devices are reviewed and some solutions for superparamagnetic interacting clusters, non-interacting beads and ferromagnetic contiguous or codebar nanowires are presented. The influence of both carrier size and transition toward the nanoscale regime on the trappability of some magnetic nanocarriers is evaluated in terms of finite-length Navier boundary conditions and applied in order to compare the motion of superparamagnetic beads and ferromagnetic nanowires in conventional continuous-flow magnetic confinement devices.

Keywords: magnetic nanocarriers, magnetic nanostructures, ferromagnetic nanowires, superparamagnetic beads, codebar nanowires, microfluidics, saturation field, FORC, magnetic manipulation

Reference for publisher use only

1 Introduction

The synthesis of the magnetic nanostructures especially magnetic nanoparticles and nanowires has been fuelled by their potential as carriers in biological applications. A special interest has been paid to their use in drug delivery, magnetic resonance imaging (MRI), nano-heating and sorting, purification or filtering of biological species using magnetic separation of bio-molecules grafted on magnetic carriers [1-3]. The efficiency of magnetic separation and manipulation of these carriers relies mainly upon two factors: i) the amount of the magnetic driven force acting upon them and, ii) the capture efficiency of bio-molecules on the surface of the carriers which is mainly related to the efficiency, specificity and the stability of the chemical functionalization on the carrier surface.

Recently, microsystems offering this functionality have been reported [4-25]. Since the magnetic forces acting upon magnetic nanocarriers depend not only on their intrinsic magnetic properties but on both magnetic field intensity and gradient, accurate knowledge about the fields generated by integrated micro-electromagnets has to be obtained in order to design efficient confinement devices. Although analytical approaches to the modeling of simple or periodic electromagnets may be employed [26], the use of numerical techniques for solving the corresponding Maxwell equations [27] is suitable for magnetic field optimization especially when more complex trapping configurations are used [18, 28]. Additionally, magnetic manipulation in microdevices requires nanocarriers which do not agglomerate in the absence of applied magnetic fields while providing enough trapping efficiency under confined magnetic fields. As superparamagnetic particles do not exhibit remanent magnetic moment and are commercially available, most part of the applications in the last years use exclusively micron- or submicron-sized superparamagnetic carriers [4, 5, 8, 12, 13, 18, 24, 25, 28-37]. However, as the dimensions of these carriers reduce under 100 nm, important limitations in the efficiency of the magnetic trapping may occur mainly due to the diminution of the magnetic moment per carrier. Thus the design and synthesis of new magnetic carriers with enhanced magnetic moment such as clusters of superparmagnetic nanoparticles, feromagnetic nanowires and nanodisks become of great interest but they require detailed knowledge about intrinsic physical parameters as saturation magnetization, coercive field, internal micro- and micromagnetic structure. Despite the fact that single ferromagnetic nanoparticules may be characterized by Magneto-optical Kerr Effect (MOKE) [38] or polarized MOKE [39], statistical approaches [40-45] based upon measurements of arrays or assemblages of these particles may often be more effective as the magnetic nanocarriers for biological applications need to be synthesized on a large scale using either colloidal chemistry for nanoparticles or template synthesis for nanowires.

Since the manipulation in microfluidic devices used in biomedical applications involve liquids, a very special attention has to be paid to Navier-Stokes equations for laminar flows in ducts [46, 47]. As the geometry of microchannels is generally regular (circular or rectangular pipes), analytical solutions of these equations are often available [46, 47]. However, as the dimensions of these devices diminish, important deviations from both Newtonian behavior and no-slip approximation for the boundary conditions may occur [48] and have to be taken into account.

Another important problem related to Navier-Stokes equations consists of evaluating the drag force acting upon the nanocarriers. Obviously, the difficulty of this problem is raised by the boundary condition at the nanoparticle surface and a complete molecular dynamics approach to the drag has to be considered [49]. However, classical approaches based upon Navier-type boundary conditions [50, 51] may provide useful and simple

analytical expressions for the drag force for carriers of regular shapes (spheres, cylinders or spheroids). The theoretical aspects related to the drag force reduction for carriers of arbitrary shape at the nanoscale regime becomes of increasingly importance as new types of passive [52] and active [53-55] magnetic nanocarriers were demonstrated to be useful in biomedical applications.

Several research and review papers on the manipulation of superparamagnetic beads in microfluidic devices [29, 32, 33, 35, 56, 57], bio-functionalization of magnetic beads [13, 30, 58, 59], modeling of magnetophoretic systems [17, 37, 60-62] or accurate techniques for the detection of targets [19, 63-68] have been published in the past years. In this paper we present a critical analysis of the problems related to the use of existing magnetic nanocarriers for magnetic manipulation in microfluidics and extend further on the problem of the design, synthesis and characterization of new magnetic nanocarriers with potential for enhanced manipulation in microfluidic environment. Mathematical models for the motion of micro- and nano-carriers in fluids at low Reynolds numbers are also reviewed here and results of numerical simulations for magnetic trapping efficiency in continuous-flow microfluidic devices are presented.

The paper is organized as follows. Section 2 describes the experimental details of the methods typically used for synthesis of superparamagnetic nanoparticles and ferromagnetic nanowires. Section 3 presents a general introduction in micromagnetics followed by a review of some theoretical models used for the magnetization processes in superparamagnetic particles (subsection 3.2) and ferromagnetic nanowires (subsection 3.3). Subsection 3.4 presents an analytical model for the remanent magnetization states in small cylindrical ferromagnetic particles. This model is then used to estimate nanowires interactions in aqueous solutions and compute the agglomeration time for various concentrations of the colloidal suspensions. Finally, the Section 4 is dedicated to magnetic manipulation of the magnetic particles in micro-devices and presents recent theoretical and experimental studies performed by our group on the manipulation of magnetic carriers in magnetic confinement devices.

2 Magnetic nano-carriers synthesis

In this section, we present some experimental methods of preparation of magnetic carriers for bio-medical applications. The state-of-the-art techniques for the fabrication of these carriers are reviewed and some results obtained by our research group in the fabrication of model systems (superparamagnetic nanoparticles, ferromagnetic contiguous or multi-segmented nanowires) used for magnetic manipulation experiments and validation of theoretical models are presented.

2.1 Superparamagnetic nanoparticles

Magnetic nanoparticles (NPs) are one of the most important and widely used magnetic nano-materials due to their potential for a variety of applications spanning from magnetic recording media, drug-targeting delivery, cell labeling and sorting, magnetic resonance imaging, separation and enrichment of even a trace amount of biospecies [30, 69, 70]. For these applications, especially biological ones, NPs with controlled size, shape and size distribution, and surface properties are necessary in order to have uniform and reproducible physical and chemical properties. One of the most important properties that makes the small magnetic nanoparticles very attractive for biological applications is theirs superparamagnetic behavior. When the size of the particles decreases below a critical value, generally less than 15 nm, each nanoparticle exhibits superparamagnetism if the temperature is above the blocking temperature. Each individual nanoparticle has a large constant magnetic moment and behaves like a giant paramagnetic atom showing no

magnetic moment in the absence of any applied magnetic field and negligible remanence and coercivity on their major hysteresis loops.

Important requirements for efficient magnetic manipulation of these NPs in applications using magnetic separation are high magnetic moments as well as very good size uniformity. Most of the experimental research until now has been dedicated to the synthesis of Fe_3O_4 nanoparticles with a relatively low saturation magnetization. However, in search for carriers with higher magnetic moment, binary alloys of CoFe have been recently considered [71] due to their increased saturation magnetization. As expected form the Slatter-Pauling curve, $Fe_{70}Co_{30}$ exhibit the highest magnetization of all binary ferromagnetic alloys and, as pointed out by Reiss [72], the force created on $Fe_{70}Co_{30}$ NP's exceeds that on Fe_3O_4 by more than one order of magnitude. This can provide the possibility to design and synthesize carriers with enhanced magnetic moment and consequently increased mobility under external magnetic filed.

Other important requirements are the physical and chemical stability as well as the possibility to functionalize the surfaces with molecules that can provide appropriate specificity to biological or chemical targets. This often requires the synthesis of core-shell architectures with magnetic core and organic or inorganic shell. The most commonly used superparamagnetic NP's are the iron oxides (magnetite and maghemite) prepared by high temperature decomposition of iron organometallic compounds [73-77]. The bare iron oxide NPs are usually hydrophobic, and in many cases, they can not be directly used due to both biocompatibility and toxicity concerns, and limitations in surface functionalization as well [78-83]. To address these problems, overcoating of an inert layer such as polymer [84], gold [85-88], silver [89], or silica [90-94] onto the surface of as prepared iron oxide NPs, has already been developed. For magnetic nanoparticles, the difficulty of forming single core-shell nanostructures is largely increased as a result of magnetic interparticle interactions. In many cases, the magnetic cores are in fact clusters of many magnetic nanoparticles [95-97] whose mutual interactions can strongly influence the magnetic behavior of each cluster or even cause the loss of the superparamagnetic behavior. Therefore, controlled synthesis is the key aspect for achieving desired properties. In contrast to larger efforts aimed to synthesize magnetic core-shell nanoparticles, much less systematic work has been done to investigate the magnetic properties of the resulting core-shell hybrid structures [98, 99]. It is noted that commercial NPs with broad size distribution were often used as seeds to form SiO_2 shells. Considering the importance of the surface coating on the magnetic properties, a detailed and systematic work is desired for the biological applications of these core/shell magnetic NPs.

Fe_3O_4 NPs with average diameters of 5 nm and 15 nm were synthesized using the protocols proposed by Sun [74] and Woo[75]. To synthesize 5 nm Fe_3O_4 NPs, $Fe(acac)_3$ (2 mmol), 1,2-hexadecanediol (10 mmol), oleic acid (6 mmol), oleylamine (6 mmol), and phenyl ether (20 mL) were mixed and magnetically stirred in a three neck 100 ml glass flask under nitrogen protection. For the preparation of Fe_3O_4 NPs with larger diameter (15 nm), $Fe(CO)_5$ 0.4 ml (3.04 mmol) was injected rapidly into a mixture containing 20 ml of octyl ether and 2.5 ml of oleic acid at 100 °C. The resulting mixture was slowly heated to 285 °C for 2 h. During the heating process, the color of the reaction mixture changed from brown, to colorless and then to black. The reaction mixture was then cooled down to the room temperature followed by precipitation and purification similar to that for the 5 nm Fe_3O_4 NPs. TEM images of these NPs in Figure 1.(a) and (c) show high quality NPs with well controlled size, shape, and narrow size distribution. The sizes of the two kinds of NPs are estimated from these measurements to be 5 nm and 15 nm NPs, respectively. Figure 1.(b) and (d) show TEM images of NPs of 5 nm and 15 nm diameter after coating with shells of Au and SiO_2, respectively.

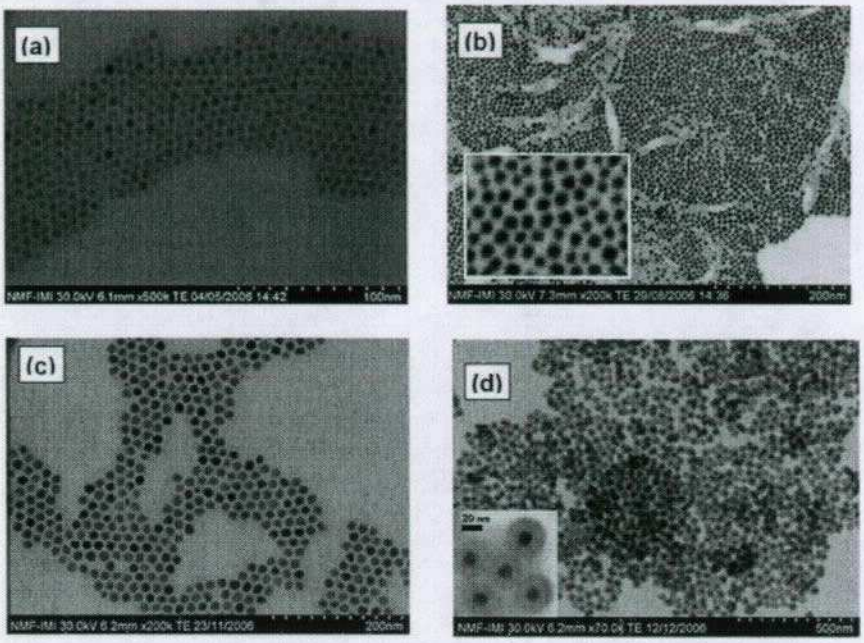

Figure 1 TEM images of 5 nm bare Fe_3O_4 nanoparticles (a) and then covered with 2nm Au shell (b). 15 nm bare Fe_3O_4 nanoparticles prior to SiO2 coating (c) and after 15 nm SiO2 shell coating (d).

The formation of the Au shell was performed following a protocol proposed by Wang et al. [85]. Figure 1.(c) shows TEM images of the 5 nm Fe_3O_4 NPs after gold-coating. A comparison between the bare Fe_3O_4 NPs and Au-coated ones show that after the metal coating, the particles become larger (size changed from ~ 5 nm to ~ 6 nm) and darker. The formation of the Au shell onto surface of the iron oxide NPs was confirmed by UV-vis spectra revealing the plasmon band of the gold shell as shown in Figure 2.(a).

The silica-coated Fe_3O_4 NPs were prepared according to a microemulsion route reported by Yi et al. [90]. Figure 1.(d) shows the results after coating with approximately 15 nm of SiO2 shell. For this synthesis, 0.24 g Polyoxy-ethylene(5)nonylphenyl ether (0.56 mmol, Igepal CO-520) was dispersed in cyclohexane (4.2 mL) by sonication. 300 µL cyclohexane solution (0.8 mg/mL of cyclohexane) was then added and the resulting mixture was vortexed followed by the addition of ammonium hydroxide (29.4%, 35 µL).

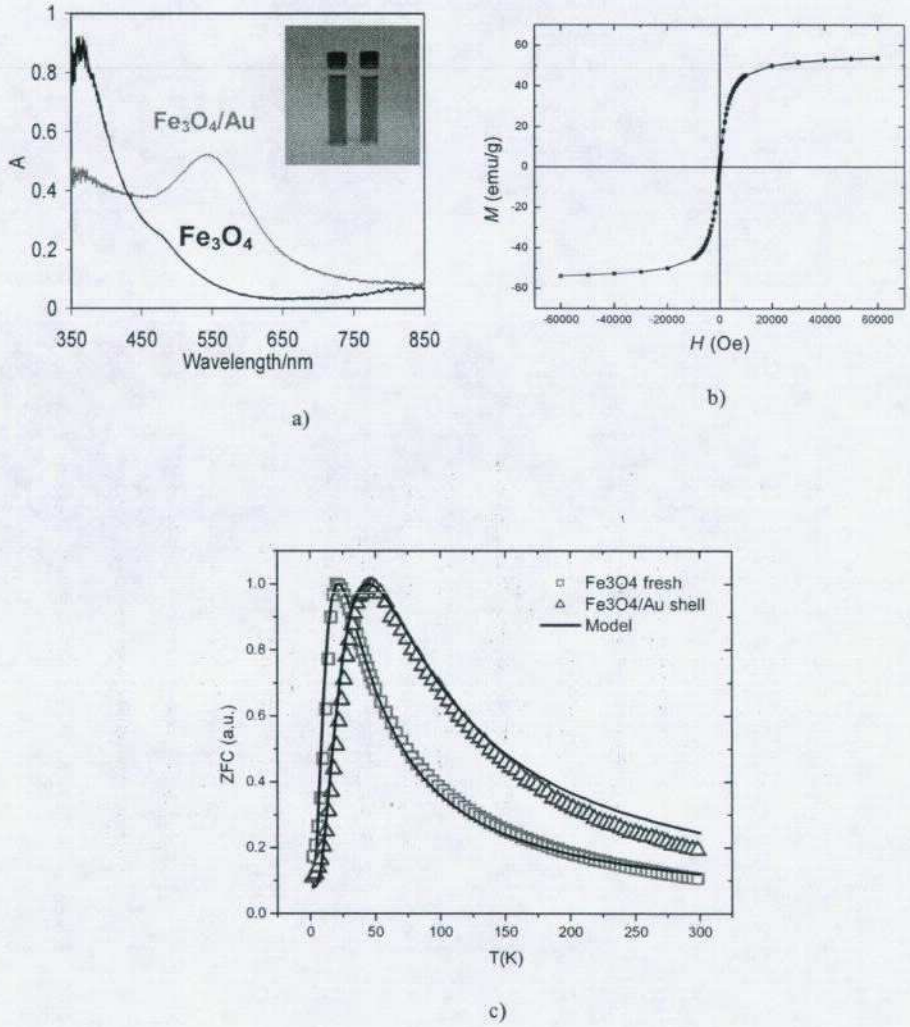

Figure 2 (a) UV-vis spectra of 5 nm Fe_3O_4 NPs before and after gold-coating. Inset is photograph of hexane solutions of bare Fe_3O_4 NPs (left) and Fe_3O_4/Au core/shell NPs (right).; (b) Magnetization curve of 5 nm Fe_3O_4 nanoparticles at 300 K; (c) ZFC measurements (points) and theoretical modeling (lines) of 5 nm Fe_3O_4 NPs before and after gold-coating.

In a following step, TEOS was added, and the reaction was stirred for 24 h at room temperature. Finally, the Fe_3O_4/SiO_2 nanoparticles were precipitated by the addition of methanol was and collected by a magnet, washed with methanol, and redispersed in ethanol.

In order to evaluate the influence of various preparation methods on the magnetic behavior of the superparamagnetic NPs, absorbtion spectra (Fig. 2.a), major hysteresis

loops (Fig. 2.b) and field-dependent magnetization curves (Fig. 2.c) were measured. The magnetic measurements were performed at 300 K for magnetic fields up to 7 T for both bare and coated NPs using a Quantum Design PPMS. The major hysteresis loop of bare Fe_3O_4 nanoparticles confirms the superparamagnetic behavior of the samples. The temperature-dependent zero-field-cooled (ZFC) magnetization measurements were performed by cooling the samples down from $300\,K$ to $2\,K$ and applying a magnetic field of 50 Oe. Then, the magnetic moment of the sample was measured during the heating cycle from 10 K to 300 K. Figure 2.c) shows the ZFC curves measured on bare (squares) and gold coated (triangles) Fe_3O_4 nanoparticles. As observed in this figure, the shell play an important role in the magnetization processes of magnetic nanoparticles as the topology of the ZFC curves has changed after coating with gold although the particles have the same magnetic core. As the particle size distributions in these two samples are almost identical, the shift of the ZFC peak along the temperature axis may suggest variations of either effective anisotropies in individual nanoparticles or mutual interactions due to the modifications of interparticle distances induces by the gold shell. The influence of the shell on the magnetization processes of these particles may be evaluated by mathematical modeling of the ZFC behavior and accurate evaluations of mutual interactions between particles, as described in following sections.

2.2 Ferromagnetic nanowires

Ferromagnetic nanowires are of great technological interest and have become very promising systems for the design of high-density perpendicular recording media, logic gates, and magnetic sensors and more recently have been proposed as carrier for biological applications mainly in cell manipulation [100, 101] or pathogen diagnostics [102]. Despite their large magnetic moments which give a tremendous advantage for magnetic manipulation when compared with superparamagnetic NPs, when suspended in liquids ferromagnetic nanowires (Ni, Co, Fe or their alloys) are subjected to strong agglomeration even in the absence of any external magnetic field. In order to solve the agglomeration problem, multi-segmented nanowires composed of ferromagnetic Ni sections separated by nonmagnetic spaces (often Au, Ag or Cu) have been recently proposed [103]. The nonmagnetic spacer is used in order to tailor mutual interactions between magnetic segments of the same wire as well as between different nanowires. Tanase and coworkers [101] has demonstrated increased magnetic trappabilities using 350 nm diameters nanowires containing an 8 nm Ni section in the center and with 2-μm Pt segments at each end. Previous literature reports on the use of magnetic nanowires as carriers demonstrated enhanced efficiency in manipulation of cells or biomolecules [100-102]. However, quantitative understanding about the ways to design optimal multisegmented configurations with tailored individual geometries (diameter, length, length of the magnetic and non-magnetic segments) is still a challenge. This raises new interesting and fundamental questions about mutual interactions in dynamic configurations of nanowires which requires new characterization and modeling methods able to extract information about both intrinsic and empirical properties of individual nanowires from the collective behavior of the corresponding magnetic nanostructures. These nanostructures consisting of magnetic nanowires or multisegmented nanowires (alternating magnetic and non-magnetic regions) are in most of the cases fabricated by electrodeposition of metals (Co, Ni, Fe, Au, Ag, Cu, etc.) or their alloys into the pores of various types of templates fabricated using either anodized aluminum oxide (AAO) or lithographically patterned templates [104-108].

Our attention in this paper is mainly focused to the understanding of fundamental properties of magnetic nanowires with different sizes, diameters and compositions as well as to de design of the optimal multi-segmented architectures that

may avoid the agglomeration while providing the maximum magnetic driven force. We present below the experimental details for the fabrication of these ferromagnetic nanowires. Further on, the mathematical models used in order to extract physical properties as as well as to study the magnetic manipulation in microfluidic environments are presented in detail in Section 4.

Among various methods used for preparing nanowire arrays, the electrochemical and electroless [109] techniques for the deposition of magnetic materials in nanoporous AAO templates are very convenient approaches for producing large arrays of parallel and almost identical nanowires [110]. The homogeneity in both geometry and physical properties of these nanoparticles are very important prerequisites for any relevant biological experiments or technological use. Consequently the control of the AAO membrane fabrication able to produce uniform and reproducible pore sizes over very large area is becoming a very important issue. AAO nanoporous membranes are usualy synthesized using the two-step anodization method of high purity Al plate at constant voltage (0.3M oxalic acid, 40 V) developed by Masuda and Fukuda [111]. The method provide only a limited control over the pore spacing: 66 nm (0.3MH_2SO_4, 25V), 100 nm (0.3M oxalic acid, 40V), and 500 nm (0.1 M H_3PO_4, 195V). The ordered pore array is then obtained by self-organization and is always hexagonal close-packed. However, this method leaves an Al_2O_3 layer (barrier layer) between the porous material and the Al substrate. The process of detaching the AAO film from its Al substrate is still a challenge. Generally, the Al substrate can be removed by oxidation with $HgCl_2$ [111], $CuCl_2$ [112], or $SnCl_4$ [113], and then the remaining barrier layer is dissolved in H_3PO_4(aq) solution. After these steps, a fragile AAO film with enlarged pores is obtained. Further more, the barrier layer can also be thinned by gradually reducing the anodizing voltage. However, this is a long and not very efficient process as the resultant AAO film still presents very fine pores at its base. An electrochemical method has already been developed [114-116] for the detachment of AAO films via the application of a short, high voltage pulse to the Al anode in a perchloric acid and 2,3-butanedione solution. However, it is well known that perchloric acid is a potential explosive, and butanedione and methanol are very volatile, costly and potentially hazardous solvents.

In order to overcome these difficulties, our group has recently been developed methods for rapid and efficient detachment of the AAO nanoporous layer from the Al substrate without perchloric acid and 2,3-butanedione just by using hydrochloric acid alone. As an example, Figure 3.(a) shows the SEM images of the bottom of an AAO film having and ordered pore array with the interpore distance of 100 nm that has been separated from its Al substrate when a 45V voltage pulse was applied for 3 s in HCl aqueous solution. The degree of pore opening and removal of the barrier layer can be controlled by the acidity of solution and the applied voltage. Our process makes the detaching of AAO film easy, clean and inexpensive, with great potential for the mass fabrication and development of application of AAO films in templates deposition of nanowires. These templates were used in order to produce pure Ni, CoFe, CoFeP [44] as well as multi-segmented Ni/Au nanowires with diameters ranging from 40 nm to 100 nm and lengths from 200 nm to 40 microns. Figure 3.(b) shows an array of 20.8 μm long CoFeP nanowires having 40 nm diameter while Figure 3.(c) and Figure 3.(d) present respectively SEM and EDX images of free standing multi-segmented nanowires having 40 nm diameter, a 20 nm central Ni segments and two cap Au segments of about 200 nm each.

In an effort to understand how geometry and nature of ferromagnetic nanowires play a role on their interactions as well as on the mobility under confined magnetic fields, magnetic measurements and micromagnetic simulations have been performed and will be presented in the following sections.

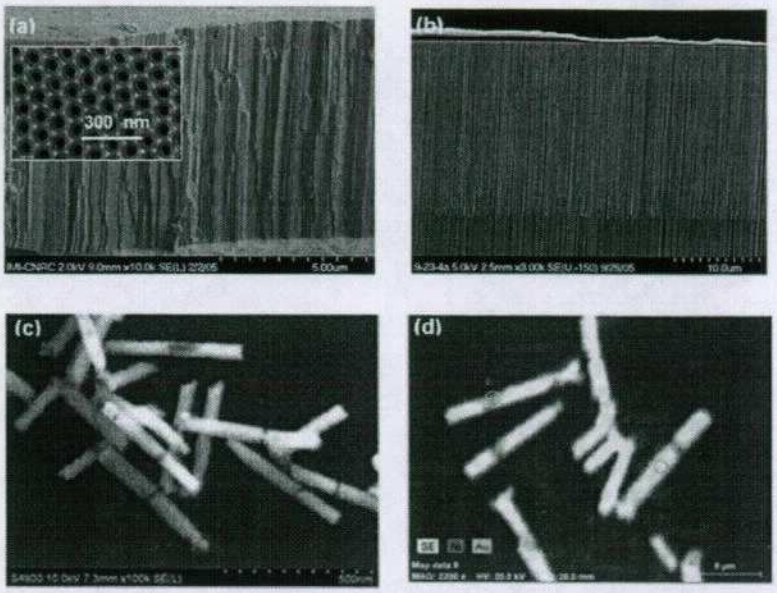

Figure 3 (a) Botom and cross-sectional views of AAO film detached by a voltage of 45 V in aqueous HCl solution with the concentration of 19.5%, howing the complete opening of a pore having 50 nm diameter. The scale bars are 300 nm; (b) Electrodeposited CoFeP nanowires with 40 nm diameter and 20.8 μm μm length (from Ref. [44]); SEM (c) and EDX (d) images of 40 nm diameter multisegmented Ni/Au nanowires prepared by electrodeposition.

3 Magnetic characterization and modeling

Intrinsic properties of magnetic nanocarriers used in separation microdevices are very important for the driven forces obtained from electromagnets. As the magnetization states of carriers may depend upon the applied magnetic field, accurate information about internal micromagnetic structure as well as applied field dependence of their magnetization states are necessary in designing carriers that can be efficiently manipulated with existing confinement devices. Recently, experiments on magnetorotation [117] or magnetic manipulation [100, 118] of ferromagnetic nanowires proved significant potential advantages over commercially available magnetic particles. However, the use of ferromagnetic nanoparticles instead of superparamagnetic beads may induce some additional problems related to mutual interactions [100] and consequently agglomerations in clusters especially when suspended in low viscous liquids. This inconvenience may be overcome by a better design of both individual carriers and confinement device so that the agglomeration time is much smaller than the experiment time.

Since the magnetic moment of the magnetic nanocarriers is responsible for the imposed field magnetic interactions and consequently the magnetic driven force, accurate knowledge about the remanent magnetization states of these carriers is needed. Moreover, as magnetization processes in ferromagnetic materials are strongly non-linear, the dependence of the magnetic configurations on the magnetic field generated by the confinement or manipulation devices has to be accurately analyzed. We review in this

section the basic concepts related to the modeling of both equilibrium magnetization states and magnetic forces acting upon magnetic nanocarriers subjected to applied magnetic fields. Then we present one of the most used theoretical approaches for the modeling of ZFC magnetization processes of assemblies of superparamagnetic nanoparticles. Then we continue with some more general methods, that can be used for either superparamagnetic or ferromagnetic nanoparticles such as first order reversal curves (FORC) or partial FORC (pFORC). Micromagnetic algorithms for the magnetization state of individual ferromagnetic nanoparticles and analytical models for the remanent magnetization states in ferromagnetic nanocylinders are presented as well, the main objective being to find the magnetic force acting upon individual carriers in known magnetic field configurations.

3.1 General micromagnetics

The fundamental problem in micromagnetism is to find the magnetization vector $\vec{M}$ of a rigid body Ω subjected to the Heisenberg-Weiss constraint $|\vec{M}| = M_s$ everywhere in Ω so that the Gibbs functional

$$E[\vec{M}] = E_{EX}[\vec{M}] + E_D[\vec{M}] + E_Z[\vec{M}] \quad (1)$$

presents a minimum, where E_{EX}, E_D and E_Z in Eq. (1) are respectively the exchange, demagnetization and Zeeman energies [119].

Analytical micromagnetism deals with analytical expressions of the above energetic terms and their derivatives but this approach is relatively limited in both particle geometry and accuracy of the obtained solutions even when simple ferromagnetic shapes as spheres or cylinders are to be analyzed. A much powerful approach to the minimization of the Gibbs functional F is purely numerical and consists of discretizing the domain Ω in small cells (elements) and replace the minimization of F with the equivalent condition [119]

$$\vec{M} \times \vec{H}_{eff} = 0 \quad (2)$$

where $\vec{H}_{eff}$ is the effective field in each cell of the mesh.The cells are successively scanned and the condition (2) fulfilled by appropriate adjustments of the direction of $\vec{M}$. The equilibrium state is then obtained when no adjustments of the directions of $\vec{M}$ in all the cells of the mesh are necessary in order to fulfill Eq. (2). The most difficult part in any micromagnetic code is related to the computation of the demagnetization energy E_D because of the long-range character of the magnetic interaction. Since the demagnetization field at a given point of the mesh has to be obtained from the contributions of all N cells of the mesh, a very inconvenient increasing of the computational efforts with N^2 is obtained. In order to overcome this difficulty, the demagnetization field is usually computed by using either a hybrid boundary element/finite element scheme [120, 121] or the Fast Multipole Method (FMM) [122]. These improvements to the reduction of the computational time in the evaluation of the demagnetizing field allowed in last years the development of various numerical software for micromagnetic calculations [123, 124].

Despite their relatively small dimensions, the ferromagnetic nanocarriers used in biomedical applications still contain a large number of atoms so that the quantum-physical description of the matter may be neglected in a first approximation and continuum approaches - as the theory of micromagnetism [119] described above– be still

valid (see Ref. [125] and the references therein for recent reviews of the state-of-the-art mathematical techniques in micromagnetism).

Since the magnetization vector field $\vec{M}$ in magnetic nanoparticles may be strongly nonuniform (magnetic moments may have different orientations from cell to cell), the magnetic force acting upon such objects has to be evaluated by accounting for the contributions from each cell of the mesh i.e.

$$\vec{F}_2 = \mu_0 \sum_i (\vec{m}_i \nabla) \vec{H} \tag{3}$$

where $\vec{m}_i$ is the magnetic moment of the cell i. Despite the obvious advantage of the accuracy in evaluation of the magnetic driven force, the expression (3) present a serious numerical inconvenient when the modeling of mutual interactions between particles is envisaged: if each particle of an interacting system of n particles if provided with a mesh of N cells, the computational effort is of the tremendous order $O(N^2 n^2)$. Obviously, in this kind of applications more simple representations of the magnetization states in applied magnetic field are needed. As we shall see in Section 3.4, remanent states in amorphous ferromagnetic cylindrical carriers may accurately be represented by simple analytical functions and the calculation of $\vec{F}_2$ much more simplified.

Magnetization states in superparamagnetic particles are relatively simple to model as their average magnetization $\vec{M}$ is generally proportional to the applied magnetic field $\vec{H}$

$$\vec{M} = \chi \vec{H}\,, \tag{4}$$

the proportionality constant χ between these two quantities being the magnetic susceptibility. So in applied magnetic field superparamagnetic particles are uniformly magnetized and we can simplify Eq. (3) by considering that all $\vec{m}_i$ are parallel to the external applied magnetic field. Using this result, we can easily express the magnetic force acting upon such a particle as [126]

$$\vec{F} = 2\pi\mu_0 R^3 \frac{\chi}{\chi + 3} \nabla \vec{H}^2 \tag{5}$$

where R is the particle radius.

Magnetic forces acting upon ferromagnetic nanowires are more difficult to model as their magnetic configurations are more complicated than those in superparamagnetic beads especially as the nanowires get shorter. By numerical minimizations of the functional E in Eq. (1) one may obtain the micromagnetic configuration of the nanowire and consequently its total magnetic moment $\vec{\mathrm{M}}$. In a first approximation the nanowires can then be modeled as single magnetic cells of magnetic moment $\vec{\mathrm{M}}$ and the magnetic actuation force in applied magnetic field found with Eq. (3). For example, when magnetic moments $\vec{\mathrm{M}}$ are parallel to the magnetic field $\vec{H} = H \cdot \hat{h}$, this force may be expressed as

$$\vec{F}_{mag} = \mu_0 \left|\vec{\mathrm{M}}\right| (\hat{h} \cdot \nabla) \vec{H}\,. \tag{6}$$

Due to the relatively large values of the coercive fields, the micromagnetic structures of ferromagnetic nanowires hardly change under the influence of the magnetic field generated by conventional micro-electromagnets ($\chi \approx 0$). Then, since ferromagnetic carriers exhibit permanent magnetic moment, the magnetic manipulation device may need to provide a strong magnetic field gradient in order to achieve large values of the magnetic forces. The design of a magnetic device for this type of carriers has to rely

rather upon ferromagnetic microposts with sharp edges than microcoils carrying strong electrical currents, as the magnetic field intensity does not account for the magnetic driven force. However, as the magnetic moments of individual particles are increased, additional problems related to the interparticle magnetic interactions and consequently agglomerations may occur. The theoretical study of these mutual interactions requires more accurate analytical representations of the equilibrium magnetic states of the ferromagnetic nano-objects as the magnetic field near these nanoobjects may be very different with respect to the crude dipolar approximation [127]. Moreover, as we shall see in Section 3.4, higher order polar representations may be more adequate for large scale micromagnetic simulations.

3.2 Small particles magnetism

A very fast and convenient magnetic characterization procedure for small magnetic particles may be achieved by ZFC magnetization measurements. A ZFC measurement starts by cooling down the sample to a very low temperature (usually about $5K$) and applying a static and uniform magnetic field H. Then the temperature is quasistatically raised in steps and the magnetic moment of the sample evaluated at each value of the temperature. The temperature dependence of the magnetic moment obtained under these circumstances usually presents a peak at a value of the temperature commonly referred to as the "blocking temperature" T_B of the sample and generally related to the anisotropy barriers in individual magnetic particles [128]. However, several experimental studies [129-132] infirmed this simple interpretation of T_B and more accurate theoretical models along with new measurements protocols were proposed in order to overcome this difficulty [130, 131, 133].

Basically, two different main approaches to the modeling of ZFC processes are available: a quantum approach in which each particle is considered as a system of interacting spins described by the Heisenberg Hamiltonian [134, 135] or, a classical approach, in which individual nanoparticles are considered as classical single-domain particles [133, 136-138] and their magnetization processes (especially the energy barrier) described by the Stoner-Wohlfarth model [139]. Although the quantum approach may give a deeper insight into the physical processes governing the superparamagnetic behavior of magnetic nanoparticles, the classical method is more effective when large statistical distributions of magnetic nanoparticles have to be characterized and therefore it will be described further bellow.

As the dimensions of superparamagnetic particles may range from a few nanometers to a few tens of nanometers, the surface-to-volume ratio increases dramatically and surface effects may play a very important role in the magnetic behavior of the sample. A physical quantity that may be considered in describing this kind of phenomena is the surface anisotropy k_S. When uniaxial anisotropy k_u for individual nanoparticles is considered, a total anisotropy constant expressed as

$$K_{eff} = K_u + K_S \tag{7}$$

may be considered in order to distinguish between bulk and surface contributions to magnetization processes of the sample.

Magnetic particles are considered either as "blocked" if thermal effects are weak compared to the magnetic energy barrier $U(H)$ needed for magnetization reversal or "deblocked" otherwise. The threshold temperature T_B responsible for the transition of particles from blocked to deblocked magnetization states may be expressed as [140]

$$T_B = \frac{U(H)}{28k_B} \tag{8}$$

where

$$U(H) = K_{eff}V\left(1-\frac{H}{H_c}\right)^{\alpha}. \tag{9}$$

V in the expression above is the particle volume, H_c is the coercive field, k_B the Boltzmann constant and α a phenomenological parameter often approximated with 1.5 in systems characterized by random orientations of the easy axes of the particles [133]. According to Wohlfarth [140] the magnetic susceptibility of individual magnetic particles in a superparamagnetic assemble is

$$\chi = \frac{\mu_0 M_s^2}{3} \times \begin{cases} K_{eff}^{-1}, & T < T_B \\ \dfrac{V}{k_B T}, & T \geq T_B \end{cases} \tag{10}$$

where T is the temperature of the sample, μ_0 the well known vacuum permeability and M_s the saturation magnetization of the magnetic material. With Eq. (10) it is straightforward now to find the total magnetic moment as the sum of two contributions from blocked ($T < T_B$) and deblocked ($T > T_B$) particles

$$m_{ZFC}(T;H) = \mu_0 M_s^2 H V_{tot}\left[\frac{1}{3K_{eff}}\Gamma_3(D;D_b,\infty) + \frac{\pi}{18k_B T}\Gamma_6(D;0,D_b)\right] \tag{11}$$

where the notation

$$\Gamma_n(D;a,b) = \frac{\int_a^b D^n f(D)dD}{\int_0^\infty D^3 f(D)dD}. \tag{12}$$

was employed. $f(D)$ is usually a log-normal function and represent the diameter (D) distribution of the particles whereas D_b is a temperature-dependent parameter deduced from Eqs. (8) and (9) and referred to as the deblocking diameter. Experimental measurement of the temperature dependence of m_{ZFC} are interpolated in the least square sense with Eq. (11) and the parameters of interest (usually K_{eff}) extracted from this interpolation. Surface contributions to the magnetization processes are then evaluated by the difference between the obtained K_{eff} and the bulk anisotropy constant K_u. We present such a fit in Figure 2.c) for an assembly of FeO magnetic nanoparticles whose diameters are log-normally distributed around $D_0 = 5.5nm$. Magnetic measurements of these particles were made in uniformly increasing temperatures from $3K$ to $300K$ and a constant applied magnetic field of $4kA/m$. Since the bulk anistropy constant for these particles is about $0.6\times10^5 J/m^3$ (according to Ref. [133]) and the obtained effective anisotropy for these particles is $0.4\times10^5 J/m^3$ we may deduce that in the absence of mutual interparticle interactions additional contributions to the effective anisotropy constant from the particles' surfaces may be present in this sample. However, such an

assumption is valid only if all other factors related to the interparticle interactions may be eliminated.

The interparticle interactions are usually taken into account in a mean-field approach, by replacing the temperature T in Eq. (11) by an "apparent" temperature [141]

$$T_a = T + T^* \tag{13}$$

where T^* is a phenomenological parameter proportional to the energy density of the dipolar interactions between particles. Experimental studies of dipolar interactions in superparamagnetic assemblies [142] shown a dependence of the magnetic behavior on the system dimensionality. However, accurate numerical micromagnetic studies of the effect of dimensionality on the equilibrium magnetic state of a superparamagnetic cluster of particles [41] shown that for volume (3D) distributions of particles the effect of the magnetostatic (dipolar) interactions may be neglected (Figure 4) with a good approximation so that $T^* \approx 0$. On the contrary, extended (2D) sheets or (1D) chains may present important dimensionality dependences (up to 18%) of their magnetization state and consequently the parameter T^* is expected to have a non-negligible contribution. Other types of mutual interactions as the exchange coupling between neighbor particles are more difficult to be taken into account and a numerical micromagnetic approaches has to be considered [143].

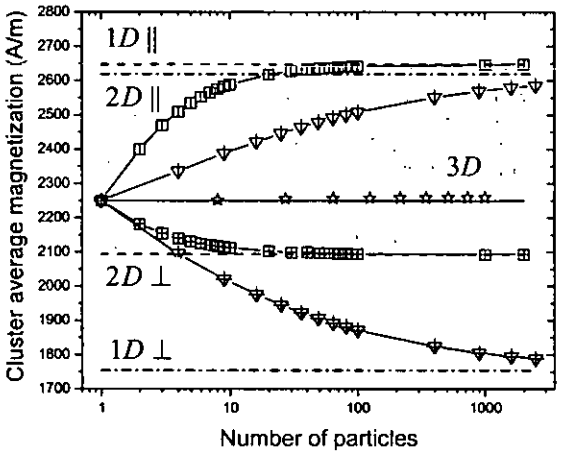

Figure 4 Partial First Order Reversal Curve (pFORC) measurement and control points (a) and distribution of switching fields in electrodeposited CoFeP nanowire arrays at pH=3.2 (b). (From Ref. [43])

The model described in this section is very appropriate for assemblies of small magnetic particles that, at a well defined temperature, undergo a transition between blocked (ferromagnetic) and deblocked (superpamagnetic) quantum states. Despite their small sizes, ferromagnetic nanowires present enhanced anisotropies along the symmetry axis mainly due to their 1D dimensionality and consequently, their deblocking temperatures may surpass the critical Curie temperature of the ferromagnetic material. So ZFC measurements of these systems can not provide useful information about intrinsic properties of individual nanowires and different approaches to the characterization of

these systems have to be employed. One of the most effective and useful characterization method, intensively used in the last years for the identification of intrinsic properties in ferromagnetic nanostructures, is the First Order Reversal Curve (FORC) diagram and will be presented in the next subsection.

3.3 Magnetization processes in ferromagnetic nanowires

First order reversal curve (FORC) method [144, 145] was initially designed as a experimental tool for the non-parametrical identification of the Classical Preisach Model (CPM) [145, 146] and intensively used in the last years for the characterization of hysteretic nanoparticulate media [147-152]. Compared to other methods, FORC diagrams may provide incredibly accurate information about either intrinsic properties of individual particles or their mutual interactions from magnetic measurements of their assemblages. Measurements protocols [148] and mathematical algorithms [45, 148] to compute diagrams from first order reversal curves are already available in the literature of the last years. The main features that could be extracted from these measurements are the distribution of switching fields and the interaction field between individual magnetic entities and are mainly based upon the Néel interpretation of CPM [153]. Numerical micromagnetic simulations on assemblages of nanosized ferromagnetic entities with well known distributions of switching fields [147, 154, 155] or Preisach distributions [156, 157] demonstrated the accuracy of the FORC diagram method in characterizing magnetic particulate media but its limitations as well [158]. However, in the design of individual magnetic nanoparticles for biomedical applications we are interested rather in the intrinsic physical properties of these particles rather than in those of their assemblages (related to mutual interactions for example). Moreover, many assemblages of magnetic nanopaticles present FORC diagrams with certain symmetry elements (points or axes) [159] so that a large amount of both measurement and computational time may be spent in order to get redundant or obvious information from the sample.

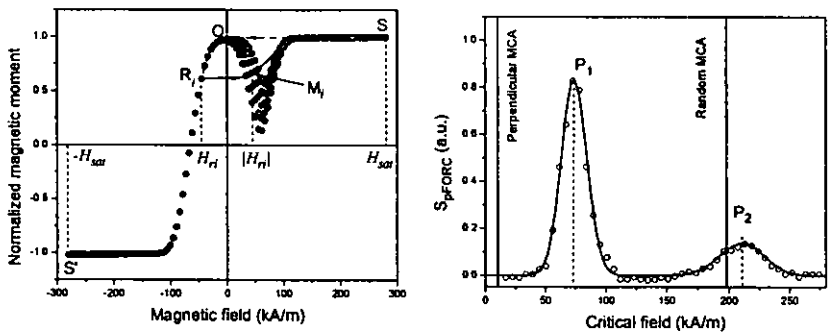

Figure 5 Numerical micromagnetic simulations of the equilibrium magnetization states in superparamagnetic assemblies (clusters) of different dimensionalities and sizes. Interrupted horizontal lines account for the analytical limits of infinite chains (1D) and infinite sheets (2D). In the absence of mutual dipolar interactions, isolated magnetic particles have a magnetization of 2250 A/m (continuous horizontal line). (From Ref. [41])

A new FORC measurement protocol designed to overcome this difficulty consists of measuring only a few points adequately chosen on each reversal curve (partial First Order Reversal Curves - pFORC) [42]. Each sample is initially saturated in strong magnetic field H_{sat} (point S in Figure 5.a) and the field ramped down to the first reversal point O corresponding to zero applied field ($H = 0$). The magnetic moment is then measured at three values of the applied field namely 0 , ΔH and $2\Delta H$ where ΔH is the field resolution (for the measurements in Figure 5.a $\Delta H = 5.6\,kA/m$ whereas $H_{sat} = 280\,kA/m$). The sample is then saturated (by applying H_{sat} again) and the field decreased to the next reversal field $-\Delta H$. Magnetic moments m are evaluated at $-\Delta H$, 0 , $+\Delta H$, $+2\Delta H$ and $+3\Delta H$ then the sample is again saturated. For a certain reversal field H_r (for example $H_{ri} = -i\Delta H$ in Figure 5), one has to evaluate the magnetic moment values at the points $(i-2)\Delta H$, $(i-1)\Delta H$, $i\Delta H$, $(i+1)\Delta H$ and $(i+2)\Delta H$ followed by successive saturations of the sample. After all partial first reversal curves have been measured, the distribution of switching fields $S_{pFORC}(H)$ is obtained by evaluating the second order mixed derivative of m with respect to H and H_r [42]

$$S_{pFORC}(H) = -\left.\frac{\partial^2 m}{\partial H \partial H_r}\right|_{H=-H_r} \qquad (14)$$

at all median points M_i of the reversal curves. An example of such an evaluation is given in Figure 5.b for measurements performed on electrodeposited CoFeP nanowire arrays at pH=3.2 following the synthesis procedure described in section 2.2 or Ref. [44]. The double-peak distribution of switching fields obtained by these measurements reveals the existence of two populations of nanowires whose intrinsic anisotropy fields are very different with respect to each other. It is obvious that when one envisages the use of these nanowires as magnetic nanocarriers in biomedical applications, the existence of nanowires with different magnetic properties may seriously affect the efficiency or even functionality of the manipulation device. Consequently, as FORC measurements may provide accurate information about both strength and distribution of anisotropies, they are strongly recommended in characterization of magnetic nanostructures whenever individual properties of individual magnetic entities play an important role in the envisaged applications. The interesting distribution revealed in Figure 5 points out that in order to get identical magnetic nanocarriers from magnetic nanostructures either additional precautions have to be considered in order to better control the synthesis process or adequate filtering devices able to select nanoparticles of interest from their arrays have to be designed. So far this feature of FORC measurements is unique and can not be easily obtained by other type of measurements.

3.4 Mutual interactions between nanowires

The cylindrical ferromagnetic nanoparticles (nanodisks and nanowires) are suitable for the use as magnetic carriers in confinement or manipulation devices as large scale fabrication techniques are already available (as pointed out in Section 2). One of the main drawbacks in the use of these carriers instead of classical superparamagnetic beads consists of the agglomeration induced by the permanent magnetic moment even in the absence of any applied magnetic field. In order to overcome this difficulty, much more attention has to be paid in the design of ferromagnetic nano-carriers in order to find a compromise between the imposed field magnetic force and the agglomeration time.

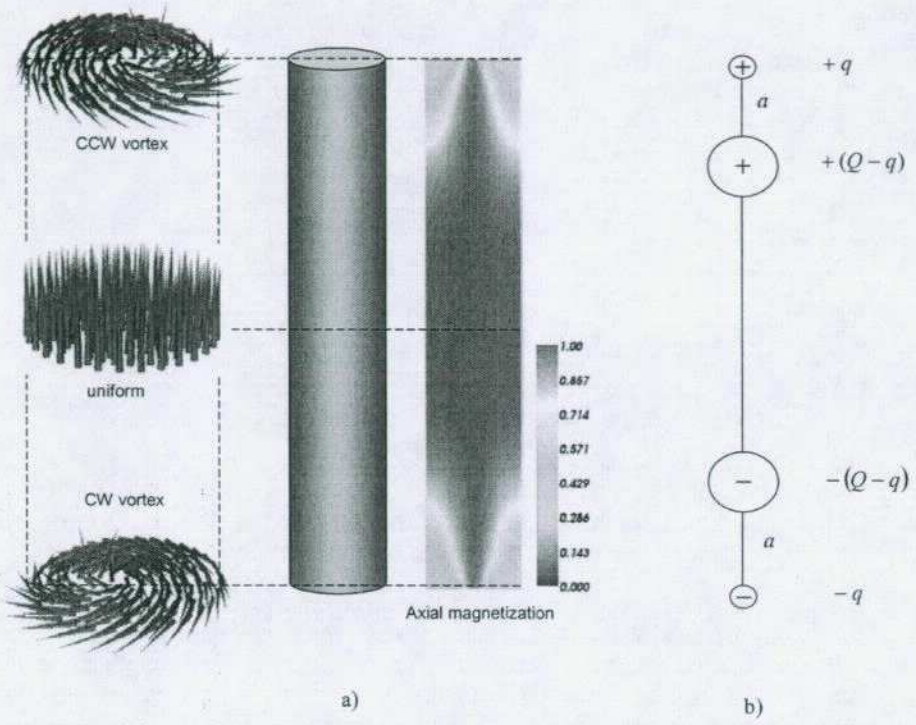

Figure 6 Remanent magnetization states in a $1-\mu m$ Ni nanowire (a) and schematic representation of the quadrupole approximation (b).

Experimental [160-162] and theoretical [163, 164] investigations of the magnetization processes in these magnetic objects revealed the existence of flux-closing vortex configurations with zero axial magnetization in the circumferential region (shell) and small regions of non-zero magnetization at the center (vortex core) [162]. As the cylinder length gets larger the remanent magnetization state evolves toward uniform magnetized states at the middle and, eventually two vortex states at the ends (Figure 6.a). By numerical micromagnetic simulations [123] we found that remanent magnetization states in cylindrical nanowires may accurately be approximated with a magnetic quadrupole (Figure 6.b) whose magnetic charges are given by $Q=\pi\left(R^2-R_v^2\right)M_s$ and $q=\pi R_v^2 M_s$ with R_v the vortex core radius, usually about $15\,nm$. The length dependence of the spacing a between q and Q at the nanowire ends is shown in Figure 7 for nanowires of $80\,nm$ radius made of different ferromagnetic materials. A good phenomenological analytical approximation to these dependences is given by

$$a(L)=a_0+\frac{k}{\sqrt{L-L_0}} \tag{15}$$

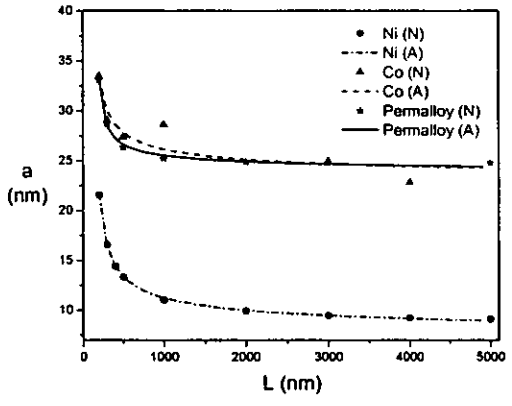

Figure 7 Length dependence of the parameter a for ferromagnetic nanowires made of Ni (diamonds), Co (triangles) and Permalloy (disks): numerical micromagnetic simulations (points) and analytical approximation (lines).

where a_0, k and L_0 are given in Table 1. Length dependences of these parameters for Ni, Co and permalloy nanowires are shown in Fig. 7. As the length of the nanowires get larger, the spacing a between the two magnetic charges at the nanowire ends stabilizes and the nanowire may be approximated with a pair of magnetic monopoles of magnetic charge $Q' = \pi R^2 M_s$ [118]. However, short segments of about $100 - nm$ length present important deviations from this crude approximation and the quadrupole model has to be employed instead.

Table 1. Numerical values of the three phenomenological parameters in Eq. (15) for cylindrical nanowires of 80 nm radius made of Ni, Co and Permalloy.

Material	$a_0(nm)$	$k(nm^{3/2})$	$L_0(nm)$
Ni	7.30	116.65	133.72
Co	22.88	38.31	109.48
Permalloy	23.66	54.82	166.6

The quadrupole approximation introduced above may simplify in a significant manner the modeling of both imposed field and mutual interactions between cylindrical ferromagnetic nano-objects by using the well known analytical expression for the magnetic field generated by a magnetic monopole Q_m

$$\vec{H} = \frac{1}{4\pi}\frac{Q_m}{r^2}\hat{r} \tag{16}$$

and the driven force acting upon it in uniform magnetic field

$$\vec{F} = \mu_0 Q_m \vec{H}\,. \tag{17}$$

In next section, we apply this approximation in order to study the magnetic interactions and the agglomeration of ferromagnetic continuous or segmented nanowires.

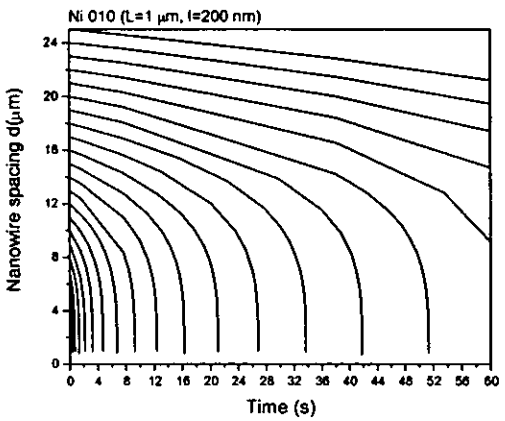

Figure 8 Time dependence of the distance between two coaxial 010 codebar nanowires in water. Each nanowire has a total length of $L = 1\,\mu m$ and contains a ferromagnetic segment of length $l = 200\,nm$ in the middle.

The simple analytical quadrupole approximation presented above allows a very simple approach to the computation of the agglomeration time for two ferromagnetic nanowires. If we consider the oversimplified case of two coaxial nanowires of length L and radius R initially at rest in a certain liquid the problem of finding the agglomeration time reduces to the differential equation of motion for one of these nanowires i.e.

$$6\pi\eta K(R,L)\frac{dx}{dt} + F_{mag}(x) = 0 \tag{18}$$

with the initial conditions $x(0) = d/2$ and $v(0) = 0$, where $K(R,L)$ is a geometrical parameter for prolate spheroids in fluids [46]

$$K(R,L) = \frac{4}{3\sqrt{\varepsilon^2 - 1}\left[\frac{1}{2}\left(\varepsilon^2 + 1\right)\ln\frac{\varepsilon + 1}{\varepsilon - 1} - \varepsilon\right]}, \quad \varepsilon = \frac{L}{\sqrt{L^2 - 4R^2}} \tag{19}$$

and $F_{mag}(x)$ the magnetic interaction force between nanowires. K in Eq. (18) equals 1 for spherical particles. The force $F_{mag}(x)$ may easily be expressed by applying Eqs. (16) and (17) for each pair of magnetic monopoles corresponding to the quadrupole representation of the two nanowires. In Figure 8 we present some solutions of Eq. (18) for two ferromagnetic codebar nanowires of length $L = 1\,\mu m$ and radius $R = 40\,nm$ with a short Ni segment of length $l = 200\,nm$ in the middle (010 codebar nanowires). As we can see in this figure, the agglomeration time for these nanowires becomes roughly about 1 min for interwire spacings about $20\,\mu m$. Obviously, the length of the magnetic segment in the codebar nanowire and the liquid viscosity as well will play a very important role in the obtained agglomeration time.

4 Manipulation of magnetic carriers in micro-devices

The integration of these technologies in micro-Total Analysis Systems (μTAS) is suitable for the detection of minute amounts of magnetically "tagged" bio-molecules since such miniaturized devices give the ability to manipulate and control volumes of fluid at the microliter or even sub-microliter scale. The characterization techniques presented in the previous sections may provide useful information about intrinsic physical parameters in individual magnetic nanoparticles. Since all the magnetic biomedical devices which use these nanoparticles as carriers must be able to provide the necessary magnetic field, the design of appropriate magnetic devices in order to generate desired profiles of the magnetic field is also very important. Moreover, along with all the requirements related to miniaturization, power consumption or magnetic materials, these devices have to provide the necessary driven force for specific magnetic particles so that their design is strictly related to the type of magnetic carriers envisaged in a given application. Ferromagnetic particles exhibit permanent magnetic moment and consequently, large values of magnetic driven forces are obtained at points characterized by strong magnetic field gradients, regardless of the magnetic field strength at those points. The corresponding magnetic devices have to rely rather upon ferromagnetic microposts with sharp edges than microcoils carrying strong electrical currents. On the contrary, as the magnetic moment of superparamagnetic particles is proportional to the applied magnetic field, both magnetic field intensity and magnetic field gradient are important for the magnetic driven force. Consequently, the presence of microcoils [26, 28, 31, 36] carried by strong electrical currents or even permanent magnets [34] that may provide strong magnetic fields becomes very important as they increase the magnetic moment of the particles and consequently the magnetic driven force [165]. Microfluidic integrated magnetic manipulation has been also demonstrated with specific designs of a magnetic device relying rather upon ferromagnetic microstructures with sharp edges coupled with the use of macroscopic permanent magnets [166, 167]. For example, in Figure 9.a) we show an array of ferromagnetic Ni posts of 100 μm diameter. When magnetized with an external permanent magnet, the Ni microposts locally concentrate the gradient of the applied magnetic field to capture the magnetic particles that are flowing above the ferromagnetic microstructures (Figure 9.b).

Although the use of permanent magnets offer great potential for continuous flow separation, they are not suitable when microscale magnetic confinement and further miniaturization or multiplexing in μTAS are required. On the contrary, micro-electromagnets carried by electrical currents not only produce strong local magnetic fields gradient but can also be easily switched on and off or can create complex static or dynamic magnetic field profiles by controlling the electrical current [26, 28, 31, 36, 168-171]. Although several electromagnetic microsystems have been developed, it is still a challenge to generate relatively large forces at the microscale to easily separate or capture magnetic particles against the hydrodynamic force. The main difficulties are related to the limitations in current densities that do not overheat the system and thus cause either the evaporation of the sample or the destruction of biomolecules. Recently, it has been proposed to combine both approaches, using ferromagnetic structures coupled with electric microcoils [18, 26]. Figure 10.a) shows a SEM image of an electromagnet composed of a gold microcoil of $50\,\mu m$ radius and square cross section whose side is about $5\,\mu m$ and a ferromagnetic Ni micropost located at the center of the microcoil and having a height of $35\,\mu m$ and a radius of $30\,\mu m$ [18].

The profile and the magnitude of both magnetic field and magnetic field gradient obtained by finite element modelling [27] near this microelectromagnet when the

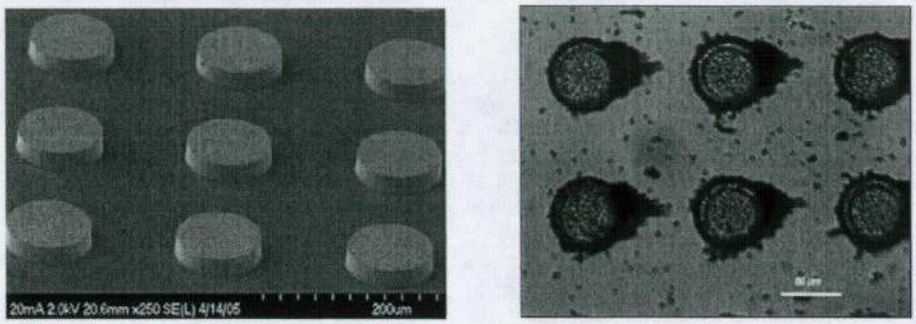

a) b)

Figure 9 a) SEM image of an array of Ni microposts fabricated at IMI; b) Optical image of magnetic capture of micron-size magnetic particles on the edges of the Ni micropost magnetized by an external magnet placed under the device.

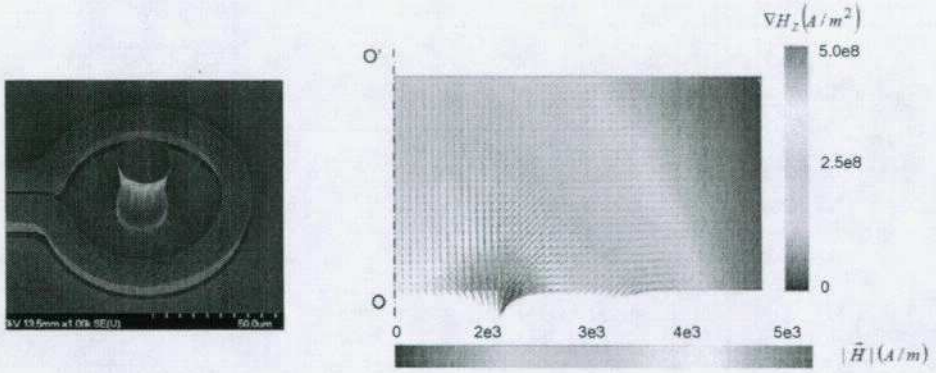

a) b)

Figure 10 a) SEM images of a microelectromagnets designed and fabricated at IMI; b) Finite element modeling of the magnetic field generated the micro-electromagnet c) in a semiplane bounded by its symmetry axis OO'. Scalar cut plane is used for $|\vec{H}|$ and vector cut plane for ∇H_z at $8\times10^8\ A/m^2$ current density carried in the microcoil.

microcoil is carrying a current density of $8\times10^8\ A/m^2$ is shown in Figure 10.b).

Several thousands of A/m for the magnetic field and tens of $10^8\ A/m^2$ for the magnetic

field gradient are typical values that may be obtained with this kind of microelectromagnets.

In order to have an insight into the magnetic actuation that can be realized with this type of microelectromagnets we present in Figure 11 a comparison of magnetic, drag and gravitational forces for 5 of typical superparamagnetic beads available commercially (Ademtech [172] and Invitrogen [173]) and ferromagnetic nanowires. The larger actuation forces obtained for micron-sized dynabeads with respect to submicron Ademtech ones rely mainly upon the larger amount of magnetic material contained in the first ones. For all the magnetic carriers under consideration here, the weight is very small compared to magnetic or drag forces and consequently inertial contributions to the particle motion may be neglected in a first approximation. However, ferromagnetic nanowires of $1\,\mu m$ length and $40\,nm$ radius may compete with the considered microbeads in these configurations of magnetic fields.

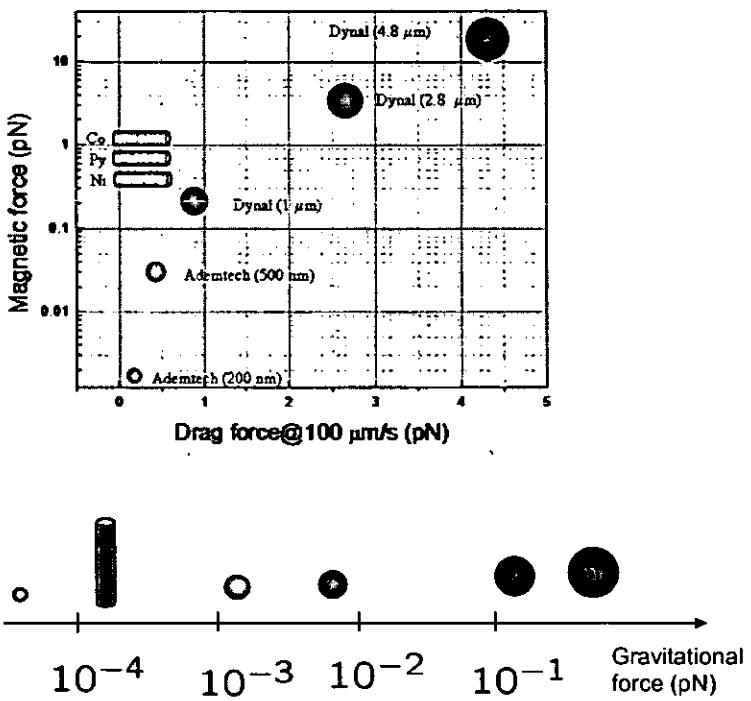

Figure 11 Gravitational, magnetic and hydrodynamic drag forces at $100\,\mu m/s$ water flow for commercial superparamagnetic beads and $1-\mu m$ length ferromagnetic nanowires in magnetic field of intensity $H = 2750\,A/m$ and magnetic field gradient $|\nabla H_z| = 1.2\times10^8\,A/m^2$.

Although Navier-Stokes equations are in general nonlinear, flow stream in microfluidic devices may accurately be described by simple, linear scalar equations[46] of Poisson type with the local liquid velocity $\vec{V}$ as unknown. Moreover, the steady flow in microfluidic channels with regular (rectangular or circular) cross sections may easily be

described by simple analytical functions [46]. For a flow between two parallel plates with no-slip boundary conditions, the liquid velocity presents a parabolic distribution known as the plane Poiseuille flow.[46] However, apart from few exceptions related to the slip boundary conditions in very narrow channels [48], the steady-state flows in microfluidic devices are well described by the no-slip boundary conditions on the channel walls.

In microfluidic flow environments, in addition to the magnetic force, the magnetic particles are subjected to drag forces. The modeling of these forces acting upon particles whose dimensions range from a few nanometers to a few tens of nanometers may rise additional problems related to the transition to the nanoscale regime [48-50, 54]. Several attempts based upon either molecular dynamics simulations [49] or classical Navier-type boundary conditions [50, 51] provided quantitative analytical expressions for the drag forces underwent by floating nanoparticles in fluid at low Reynolds numbers. According to Ref. [50] for example, the transition to total slip boundary conditions at the separation surface of nanoparticles in fluids may influence the drag force with a factor ranging from 0.66 to 1 with respect to the classical result derived from total no-slip boundary conditions. The influence of the drag force on the motion of magnetic superparamagnetic beads and ferromagnetic nanowires suspended in a Poiseuille flow near the simple micoelectromagnet described above is numerically analyzed in the following.

In the absence of any inertial contribution to the motion of micro- or nano-objects in viscous liquids, the law of motion $\vec{r}(t)$ for these particles can be obtained from the static equilibrium condition between the magnetic force $\vec{F}_{mag}$ and the drag force $\vec{F}_{drag}$ [36, 46, 56]. For spherical superparamagnetic beads this condition may be expressed as

$$0 = -6\pi\eta R\left(\dot{\vec{r}} - \vec{V}\right) + \vec{F}_{mag} \tag{20}$$

where η is the liquid viscosity, R the particle radius and $\vec{V}$ the liquid velocity. $\vec{F}_{mag}$ in the expression above represents the magnetic force acting upon the particle and is expressed as given by Eq. (5).

When ferromagnetic nanowires are employed as magnetic carriers, the drag force will depend on the nanowire orientation relative to the liquid flow and the equations of motion become more complicated than (20) as the drag force $\vec{F}_{drag}$ and the relative velocity $\dot{\vec{r}} - \vec{V}$ of the liquid flow are not collinear anymore. If we denote with $\hat{h}$ and $\hat{u}$ the unit vectors of the local magnetic field $\vec{H}$ and particle relative velocity $\vec{U}$ with respect to the liquid flow respectively, the drag force acting upon a ferromagnetic nanocylinder oriented parallel to the magnetic field direction can be written as

$$\vec{F}_{drag} = \left[-f^{\parallel}_{drag}\vec{U}\cdot\hat{h} - \sqrt{1-\left(\vec{U}\cdot\hat{h}\right)^2}\left(\hat{h}\cdot\hat{u}\right)\right]\hat{h} + f^{\perp}_{drag}\sqrt{1-\left(\vec{U}\cdot\hat{h}\right)^2}\,\hat{u}, \quad \vec{U} = \dot{\vec{r}} - \vec{V}\,. \tag{21}$$

Analytical expressions for $f^{\parallel}_{drag}$ and $f^{\perp}_{drag}$ may be obtained by approximating the cylinder with prolate spheroids or elongated rods [46, 47] whereas analytical expressions for the magnetic driven force is given by Eq. (6). As the magnetic objects reduce theirs dimensions, Navier boundary conditions must be considered at the solid-liquid interface so that Eq. (21) has to be corrected by a factor that takes into account the finite value of the slip-length at the transition toward the nanoscale regime [174].

Depending on the microfluidic flow rate, magnetic carriers floating in microfluididc channel can either be trapped by the microelectromagnetic trap (i.e. they

reach one of the walls of the microfluidic channel) or escaped when they go far away from microelectromagnet. However, for most bio-analytical applications, 100% of capture efficiency is a prerequisite for success. It is therefore primordial to be able to predict the desired magnetic trappability in minute flow microfluidic devices that can be achieved by an intelligent design of both magnetic carrier and confinement devices. The probability of capture (or trapping ratio) can be defined by

$$T = \frac{N_{trapped}}{N} \times 100\% \tag{22}$$

where $N_{trapped}$ represents the number of trapped particles and N the total number of launched particles. The equations of motion (24) are numerically solved for each object in order to determine the capture efficiency. A critical velocity V_{0c} is defined as the maximal velocity V_0 of the liquid at which only 50% of the total launched carriers fall down on the channel floor.

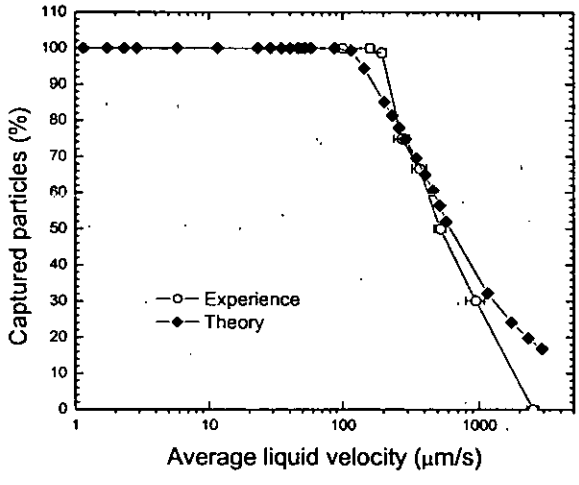

Figure 12 Capture efficiency of 4.5 µm Dynabeads for various liquid velocity using an electromagnet as described in Figure 10.a). (from Ref. [18])

In Figure 12, experimental and numerical capture efficiencies (using microelectromagnet as described in the previous section) are plotted versus flow velocity in microfluidic channel for $4.5\,\mu m$ Dynabeads. As we can see from this figure, increasing the flow velocity (i.e. the drag force) has for consequence the decrease of the capture efficiency. For the presented confinement device and magnetic carriers, simulations and experiments give the maximum velocity at $\sim 150\,\mu m \cdot s^{-1}$ in order to reach 100% capture efficiency. At higher flow rates, some particles may escape from the magnetic confinement area. This maximum flow rate is also affected by the particle size. Indeed, the reduction of the dimensions of the magnetic carriers strongly reduce the driven forces exerted on the magnetic carriers as they scale as $\propto R^3$ (R being the particle radius), while the hydrodynamic forces scale as $\propto R$ [18].

Comparisons of typical flow rates of $\mu L \cdot h^{-1}$ that were obtained in this study at 100% capture efficiency (considering the usual dimensions of microfluidic channels of thousands of μm^2) with those reported in the literature shows the limitation on the sample volumes for practical applications in terms of real-time analysis in μTAS. Although the design of the micro-electromagnetic trap could be still improved, it is clear from Figure 11 that the main limiting factor is the non-optimal magnetic properties of the actual commercial magnetic particles. Using magnetic carrier with higher saturation magnetization would help to speed up flow rates in microfluidic channels, thus reducing the time for a sample to be analyzed without affecting the efficiency of the magnetic bead capture in a microscopic volume.

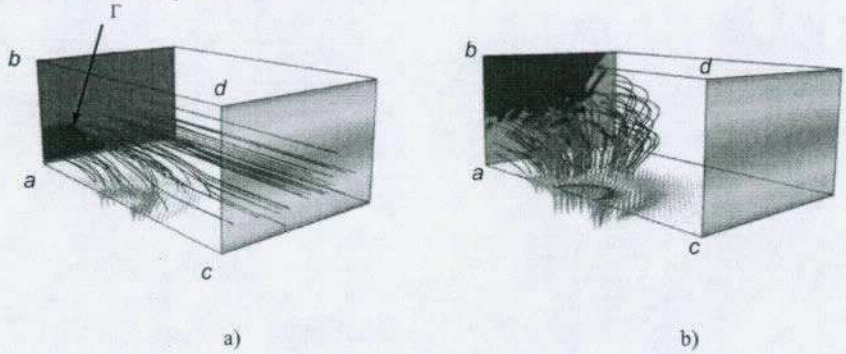

a) b)

Figure 13 Simulated trajectories of Dynabead superparamagnetic particles (a) and $1-\mu m$ length ferromagnetic nanowires (b) in a $100-\mu m/s$ water-flow microfluidic confinement device.

When ferromagnetic nanowires are considered as magnetic carriers, a huge increase of magnetic capture efficiency is expected. Numerical solutions to the equations of motion (18) and (20) are presented in Figure 13.a) and b) respectively for $100\,\mu m/s$ flow maximal velocity and a magnetic field configuration as obtained from the microelectromagnet in Figure 10.c). The superparamagnetic carriers in Figure 13.a) are Dynabeads of diameter about $1\,\mu m$ whereas the considered ferromagnetic nanoparticles in Figure 13.b) are Ni ferromagnetic nanowires of $1\,\mu m$ length and $40\,nm$ radius. If the ferromagnetic nanowires are totally confined in a physical region above the electromagnet, this is not the case with the superparamagnetic beads. The microelectromagnet seems to be less favorable to superparamagnetic beads since the magnetic field is not strong enough in order to provide these beads with magnetic moments comparable with those of ferromagnetic nanowires. Moreover, the small dimensions of the nanowires diminish the drag force thus increasing their trappability.

The effect of the drag force on the magnetic manipulation of magnetic nanocarriers may be evaluated by considering some artificial spheroidal carriers of different geometries but provided with the same magnetic moment. This kind of particles may be imagined as ferromagnetic nanowires embedded in non-magnetic prolate spheroids of uniformly increased semi-minor axes from $40\,nm$ to $500\,nm$ (Figure 14). As we may see in this figure, increasing the drag force about 120 times has as consequence an increase of the critical velocity from $1\,mm/s$ to about $6\,mm/s$ that is 6

times. As the correction factor due to the Navier boundary conditions for the drag force [50] ranges in the interval $[0.66,1]$, it is obvious that its influence on the magnetic trappability of this kind of carriers may be neglected in a first approximation. The magnetic moment of the nanocarriers have a much stronger influence on the obtained trappabilities since ferromagnetic 010 codebar nanowires of $1\,\mu m$ length (NiL100 in Figure 14) with a $100\,nm$ magnetic insertion in the middle provide a critical velocity about 10 times smaller than a $1\,\mu m$ contiguous ferromagnetic nanowire. However, even under these circumstances, the magnetic trappability is much better than that obtained with superparamagnetic beads (Dynabeads in Figure 14) as the critical velocity is only $10\,\mu m/s$ for these carriers.

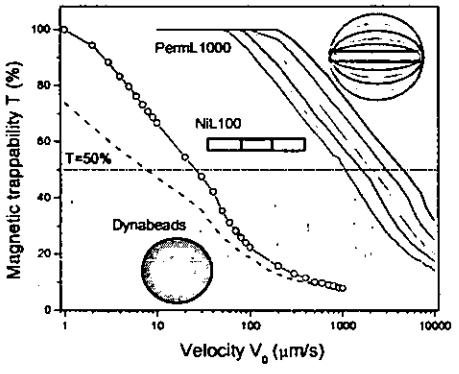

Figure 14 Dependence of the magnetic trappability T on the liquid maximal velocity V_0 for Permalloy nanowires of length $L = 1\,\mu m$ embedded in prolate non-magnetic spheroids of various radii (PermL1000), non-magnetic nanowires of $1\,\mu m$ length containing a single magnetic segment of $100\,nm$ Ni in the middle (NiL100) and commercial Dynabeads MyOne superparamagnetic microbeads of $1\,\mu m$ diameter.(From Ref. [62])

The results presented in this section show that both geometrical and physical parameters of ferromagnetic nanocarriers are very important for the magnetic manipulation in magnetic confinement devices. The desired magnetic trappability in minute flow microfluidic devices may be achieved by an intelligent design of both magnetic carrier and confinement devices.

5 Concluding remarks

In this paper, recent advances in synthesis, characterization and manipulation of magnetic carriers for biomedical applications are reviewed. After a brief presentation of the methods used for the synthesis of superparamagnetic nanoparticles and ferromagnetic nanowires, we present theoretical techniques able to extract accurate values for the intrinsic physical parameters of magnetic nano-objects from magnetic measurements of their arrays. The characterization techniques presented here may also be used in order to evaluate the homogeneity or dispersity of these nanostructures and consequently provide accurate control of the fabrication process of magnetic nanocarriers. We use analytical

and numerical micromagnetic models in order to simulate the motion of magnetic nanocarriers in liquids at very low Reynolds numbers and a very good agreement with the experimental measurements is found. In order to simplify the problem of dynamic interactions of ferromagnetic nanowires suspended in liquids, we propose a simple analytical quadrupole representation of their remanent magnetization states. This approximation greatly simplifies the computational effort in the modeling of mutual interactions between cylindrical ferromagnetic nano-objects and consequently, allows predicting how the agglomeration time depends on the structure, the geometry and nature of the magnetic material in large assemblies of interacting magnetic nanowires. Our quantitative analysis of the motion of most usual commercial magnetic carriers as well as superparamagnetic nanoparticles and nanowires subjected to magnetic field gradients generated by electromagnetic trapping configurations amendable for integration with microfluidic devices shows the potential that the nanowires can have in the magnetic manipulation if the agglomeration due to ferromagnetic interaction is overcome by a careful design of multi-segmented nanowires systems.

Acknowledgements

The authors want to thank Hélène Roberge and François Normandin for useful discussions and technical assistance in nanostrctures imaging and magnetic measurements as well as Karen Chan for assistance in nanowires preparation. We are grateful to Michel M. Dumoulin (IMI/CNRC) for his support of the functional nanomaterials program at IMI-NRC.

This work is supported by a grant from **Canadian Institutes of Health Research** and by a joint grant from the **Natural Sciences and Engineering Research Council** and the **National Research Council** of Canada.

References

1. Whitesides, G.M., R.J. Kazlauskas, and L. Josephson (1983) 'Magnetic Separations in Biotechnology', *TIBTECH*, Vol. 1, pp. 144-148.
2. Verpoorte, E. (2003) 'Beads and chips: new recipes for analysis', *Lab Chip*, Vol. 3, pp. 60N-68N.
3. Gijs, M.A.M. (2004) 'Magnetic bead handling on-chip: new opportunities for analytical applications ', *Microfluid Nanofluid*, Vol. 1, pp. 22-40.
4. Jin Woo, C., Y.W. Oh, A. Han, N. Okulan, C. Ajith Wijayawardhana, C. Lannes, S. Bhansali, K.T. Schlueter, W.R. Heineman, H.B. Halsall, J.H. Nevin, A.J. Helmicki, H. Thurman Henderson, and C.H. Ahn (2001) 'Development and characterization of microfluidic devices and systems for magnetic bead-based biochemical detection', *Biomed. Microdev.*, Vol. 3, pp. 191-200.
5. Guanxiong, L., V. Joshi, R.L. White, S.X. Wang, J.T. Kemp, C. Webb, R.W. Davis, and S. Shouheng (2003) 'Detection of single micron-sized magnetic bead and magnetic nanoparticles using spin valve sensors for biological applications', *J. Appl. Phys.*, Vol. 93, pp. 7557-7559.
6. Lee, H.Y., Y. Sacho, T. Kanki, H. Tanaka, H. Shirakawa, J.W. Cheon, J.H. Yoon, N.J. Kang, J.I. Park, and T. Kawai (2002) 'DNA-directed magnetic network formations with ferromagnetic nanoparticles', *J.Nanosci. Nanotechnol.*, Vol. 2, pp. 613-615.
7. Jwa Min, N., C.S. Thaxton, and C.A. Mirkin (2003) 'Nanoparticle-based bio-bar codes for the ultrasensitive detection of proteins', *Science*, Vol. 301, pp. 1884-1886.
8. Abe, M. and H. Handa (2004) 'Prospects for medical applications using magnetic beads in the post-genomic era', *J. Mag. Soc. Jpn.*, Vol. 28, pp. 841-846.

9. Minc, N., P. Bokov, K.B. Zeldovich, C. Futterer, J.L. Viovy, and K.D. Dorfman (2005) 'Motion of single long DNA molecules through arrays of magnetic columns', *Electrophoresis*, Vol. 26, pp. 362-375.
10. Chiou, C.H. and L. Gwo Bin (2005) 'A micromachined DNA manipulation platform for the stretching and rotation of a single DNA molecule', *J. Micromech. Microeng.*, Vol. 15, pp. 109-17.
11. Qun, G., C. Chuanding, and D.T. Haynie (2005) 'Cobalt metallization of DNA: toward magnetic nanowires', *Nanotechnology*, Vol. 16, pp. 1358-1363.
12. Bogue, R. (2005) 'Nanoparticle-based assay set to revolutionise clinical diagnostics', *Sens. Rev.*, Vol. 25, pp. 249-251.
13. Hsing, I.M. and Y. Siu Wai (2006) 'Manipulation and extraction of genomic DNA from cell lysate by functionalized magnetic particles for lab on a chip applications', *Biosens. Bioel.*, Vol. 21, pp. 989-997.
14. Hsing, I.M., Z. Wenting, and Y. Shanjing (2006) 'A microsystem compatible strategy for viable Escherichia coli detection', *Biosens. Bioel.*, Vol. 21, pp. 1163-1170.
15. Tien Li, C., T. Chien Ying, S. Chih Chen, R. Uppala, C. Chun Chi, L. Chun Hung, and C. Ping Hei (2006) 'Electrical detection of DNA using gold and magnetic nanoparticles and bio bar-code DNA between nanogap electrodes', *Microel. Eng.*, Vol. 83, pp. 1630-1633.
16. Min, L., L. Yu Cheng, and S. Kai Chun (2006) 'Using magnetic nanoparticles to enhance gene transfection on magneto-electroporation microchips', *Mater. Sci. Forum*, Vol. 505-507, pp. 661-666.
17. Piedade, M.S., L.A. Sousa, T.M. Almeida, J. Germano, B.A. da Costa, J.M. Lemos, P.P. Freitas, H.A. Ferreira, and F. Cardoso (2006) 'A new hand-held microsystem architecture for biological analysis', *IEEE Trans. Circ. Syst. I: Fundamental Theory and Applications*, Vol. 53, pp. 2384-2395.
18. Le Drogoff, B., L. Clime, and T. Veres (2007) 'The influence of magnetic carrier size on the performance of microfluidic integrated micro-electromagnetic traps', *Lab Chip*, Vol. in preparation
19. Goral, V.N., N.V. Zaytseva, and A.J. Baeumner (2006) 'Electrochemical microfluidic biosensor for the detection of nucleic acid sequences', *Lab Chip*, Vol. 6, pp. 414-421.
20. Hakho, L., L. Yong, R.M. Westervelt, and D. Ham (2006) 'IC/microfluidic hybrid system for magnetic manipulation of biological cells', *IEEE J. Solid-State Circ.*, Vol. 41, pp. 1471-1480.
21. Inglis, D.W., R. Riehn, R.H. Austin, and J.C. Sturm (2004) 'Continuous microfluidic immunomagnetic cell separation', *Appl. Phys. Lett.*, Vol. 85, pp. 5093-5095.
22. Tanaka, S., Z. Aspanut, H. Kurita, C. Toriyabe, Y. Hatuskade, and S. Katsura (2006) 'Bio-application of high-Tc SQUID magnetic sensor', *J. Magn. Magn. Mater.*, Vol. 300, pp. e315-19.
23. Wang, S.X., B. Seung Young, L. Guanxiong, S. Shouheng, R.L. White, J.T. Kemp, and C.D. Webb (2005) 'Towards a magnetic microarray for sensitive diagnostics', *J. Magn. Magn. Mater.*, Vol. 293, pp. 731-736.
24. Wang, S.X., R.L. White, G.X. Li, V. Joshi, S. Sun, D.B. Robinson, J.T. Kemp, C.D. Webb, and R.W. Davis (2003) 'Design and fabrication of bio-magnetic sensors and magnetic nanobead labels for DNA detection and identification', *Digest of INTERMAG 2003: International Magnetics Conference*, Vol. EC-01.
25. Lettieri, G.-L., A. Dodge, G. Boer, N.F. de Rooij, and E. Verpoorte (2003) 'A novel microfluidic concept for bioanalysis using freely moving beads trapped in recirculating flows', *Lab Chip*, Vol. 3, pp. 34-39.
26. Ramandan, Q., V. Samper, D.P. Poenar, and C. Yu (2006) 'Analytical model for the magnetic field and force in a magnetophoretic microsystem', *Biosens. Bioel.*, Vol. 21, pp. 1693-1702.
27. Meunier, G. (2002) *Modèles et formulations en électromagnétisme*. Hermès Science Publications, Paris.
28. Ramandan, Q., V. Samper, D. Poenar, and C. Yu (2005) 'Evaluation of current-carrying wires for manipulation of magnetic micro/nanoparticles for biomedical applications', *Int. J. Nanosci.*, Vol. 4, pp. 489-499.

29. Gijs, M.A.M. (2004) 'Magnetic bead handling on-chip: new opportunities for analytical applications', *Microfluid Nanofluid*, Vol. 1, pp. 22-40.
30. Grancharov, S.G., H. Zeng, S. Sun, S.X. Wang, S. O'Brien, C.B. Murray, J.R. Kirtley, and G.A. Held (2005) 'Bio-functionalization of monodisperse magnetic nanoparticles and their use as biomolecular labels in a magnetic tunnel junction based sensor', *J. Phys. Chem. B*, Vol. 109, pp. 13030-13035.
31. Lee, H., A.M. Purdon, and R.M. Westervelt (2004) 'Manipulation of biological cells using a microelectromagnet matrix', *Appl. Phys. Lett.*, Vol. 85, pp. 1063-1065.
32. Pankhurst, Q.A., J. Connolly, S.K. Jones, and J. Dobson (2003) 'Applications of magnetic nanoparticles in biomedicine', *J. Phys. D: Appl. Phys.*, Vol. 36, pp. R167-R181.
33. Radisic, M., R.K. Iyer, and S.K. Murthy (2006) 'Micro- and nanotechnology in cell separation', *Int. J. Nanomed.*, Vol. 1, pp. 3-14.
34. Rida, A., V. Fernandez, and M.A.M. Gijs (2003) 'Long-range transport of magnetic microbeads using simple planar coils placed in a uniform magnetostatic field', *Appl. Phys. Lett.*, Vol. 83, pp. 2396-2398.
35. Safarik, I. and M. Safarikova (2002) 'Magnetic Nanoparticles and Biosciences', *Monatshefte fur Chemie*, Vol. 133, pp. 737-759.
36. Smistrup, K., P.T. Tang, O. Hansen, and M.F. Hansen (2006) 'Microelectromagnet for magnetic manipulation in lab-on-a-chip systems', *J. Magn. Magn. Mater.*, Vol. 300, pp. 418-426.
37. Zhang, Y., R.W. Barber, and D.R. Emerson (2005) 'Particle separation in microfluidic devices - SPLITT fractionation and microfluidics', *Curr. An. Chem.*, Vol. 1, pp. 345-354.
38. Allwood, D.A., X. Gang, M.D. Cooke, and R.P. Cowburn (2003) 'Magneto-optical Kerr effect analysis of magnetic nanostructures', *J. Phys. D: Appl. Phys.*, Vol. 36, pp. 2175-82.
39. Antos, R., S. Visnovsky, J. Mistrik, and T. Yamaguchi (2005) 'Magneto-optical polar-Kerr-effect spectroscopy on 2D-periodic subwavelength arrays of magnetic dots', *Digest of 10th International Symposium on Microwave and Optical Technology ISMOT 2005*, Vol. 166.
40. Clime, L., F. Béron, P. Ciureanu, M. Ciureanu, R.W. Cochrane, and A. Yelon (2006) 'Characterization of individual ferromagnetic nanowires by in-plane magnetic measurements of arrays', *J. Magn. Magn. Mater.*, Vol. 299, pp. 487.
41. Clime, L. and T. Veres (2006) 'Numerical micromagnetics of interacting superparamagnetic nanoparticles assembled in clusters with different dimensionalities', *J. Magn. Magn. Mater. (in press)*
42. Clime, L., A. Yelon, and T. Veres (2007) 'Identification of switching fields in magnetic nanostructures by partial first order reversal curves', *J. Appl. Phys. (in review)*, Vol.
43. Clime, L., S. Zhao, F. Normandin, A. Yelon, and T. Veres (2007) 'Identification of magnetic anisotropies in arrays of ferromagnetic nanowires by partial first order reversal curves', *in preparation*
44. Zhao, S., L. Clime, C. Chan, F. Normandin, H. Roberge, A. Yelon, R.W. Cochrane, and T. Veres (2007) 'Statistical study of effective anisotropy field in ordered ferromagnetic nanowire arrays', *J. Nanosci. Nanotechnol.*, Vol. 7, pp. 1-6.
45. Clime, L., A. Stancu, P. Ciureanu, and A. Yelon (2004) 'First order reversal curve diagrams deduced by a Shepard method for bivariate interpolation of scattered data', *J. Optoel. Adv. Mater.*, Vol. 6, pp. 1005.
46. Happel, J. (1965) *Low Reynolds number hydrodynamics : with special applications to particulate media*. Prentice-Hall, Englewood Cliffs, N.J.
47. Byron Bird, R., R.C. Armstrong, and H. O. (1987) *Dynamics of polymeric liquids*. second ed. Vol. 1. John Wiley & Sons, New York.
48. Gad-al-Hak, M. (2004) 'Liquids: The holy grail of microfluidic modeling', *Physics of Fluids*, Vol. 17, pp. 100612.
49. Sirk, T., *Numerical simulations of nanoscale flow: a molecular dynamics study of drag*, in *Mechanical Engineering*. 2006, Virginia Polytechnic Institute and State University: Blacksburg.
50. Matthews, M.T. and J.M. Hill (2006) 'Flow around nanospheres and nanocylinders', *Q. Jl Mech. Appl. Math.*, Vol. 59, pp. 191-210.

51. Barber, R.W. and D.R. Emerson, *Numerical simulations of low Reynolds number slip flow past a confined microsphere*. 2001, CLRC Laboratory: Daresbury-Warrington.
52. Singh, H., P.E. Laibinis, and T.A. Hatton (2005) 'Synthesis of flexible magnetic nanowires of permanently linked core-shell magnetic beads tethered to a glass surface patterned by microcontact printing', *Nano Lett.*, Vol. 5, pp. 2149-2154.
53. Dreyfus, R., J. Baudry, M.L. Roper, M. Fermigier, H.A. Stone, and J. Bibette (2005) 'Microscopic artificial swimmers', *Nature*, Vol. 437, pp. 862-865.
54. Najafi, A. and R. Golestamian (2004) 'Simple swimmer at low Reynolds number: three linked spheres', *Phys. Rev. E*, Vol. 69, pp. 062901.
55. Gauger, E. and H. Stark (2006) 'Numerical study of a microscopic artificial swimmer', *Phys. Rev. E Stat. Nonlin. Soft Matter. Phys.*, Vol. 74, pp. 21907-1-10.
56. Pamme, N. (2006) 'Magnetism and microfluidics', *Lab Chip*, Vol. 6, pp. 24-38.
57. Safarik, I. and M. Safarikova (1999) 'Use of magetic techniques for the isollation of cells', *J. Chromatogr. B*, Vol. 722, pp. 33-53.
58. Bourlinos, A.B., S.R. Chowdhury, R. Herrera, D.D. Jiang, Q. Zhang, L.A. Archer, and E.R. Giannelis (2005) 'Functionalized nanostructures with liquid-like behavior: expanding the gallery of available nanostructures', *Adv. Func. Mat.*, Vol. 15, pp. 1285-1290.
59. Huang, P.L., R.S. Liu, H.T. Chan, Y.Y. Do, P.L. Chien, T.S. Chan, C.Y. Huang, S.Y. Yang, and H.E. Horng (2006) 'Preparation and properties of bio-compatible magnetic Fe3O4 nanoparticles', *J. Magn. Magn. Mater.*, Vol. 304, pp. e415-17.
60. Chen, S., N. Phan Thien, X.J. Fan, and B.C. Khoo (2003) 'Simulating the continuous flow separation element for DNA extraction', *Proceedings of the IASTED International Conference on Biomedical Engineering*, Vol. 84-88.
61. Furlani, E.P. and Y. Sahoo (2006) 'Analytical model for the magnetic field and force in a magnetophoretic microsystem', *J. Phys. D: Appl. Phys.*, Vol. 39, pp. 1724-1732.
62. Clime, L., B. Le Drogoff, and T. Veres (2007) 'Dynamics of Superparamagnetic and Ferromagnetic Nano-objects in Continuous-flow Microfluidic Devices', *IEEE Trans. Magn. (in press)*
63. Schwarz, M.A. and P.C. Hauser (2001) 'Recent developments in detection methods for microfabricated analytical devices', *Lab Chip*, Vol. 1, pp. 1-6.
64. Qin, J., H. Fung, Y.S. Zhu, and D.R. Lin (2004) 'Native fluorescence detection of flavin derivatives by microchip capillary electrophoresis with laser-induced fluorescence itensified charge-coupled device detection', *J. Chromatogr. A*, Vol. 1027, pp. 223-229.
65. Yang, N.Y., C. Li, J. Kameoka, K.H. Lee, and H.G. Craighead (2005) 'A polymeric microchip with integrated tips and in situ polymerized monolith for electrospray mass spectroscopy', *Lab Chip*, Vol. 869-876.
66. Benetton, S., J. Kameoka, A.M. Tan, T. Wachs, H. Craighead, and J.D. Henion (2003) 'Chip-based P450 drug metabolism coupled to electrospray ion-zation-mass spectrometry detection', *Anal. Chem.*, Vol. 75, pp. 6430-6436.
67. Liu, B.F., M. Ozaki, H. Hisamoto, Q.M. Luo, Y. Utsumi, T. Hattori, and S. Terabe (2005) 'Microfluidic chip toward cellular ATP and ATP-conjugated metabolic analysis with bioluminescence detection', *Anal. Chem.*, Vol. 77, pp. 573-578.
68. Sato, K., M. Yamanaka, and T. Hagino (2004) 'Mocrochip-based enzyme-linked immunosorbent assay (microELISA) system with thermal lens detection', *Lab Chip*, Vol. 4, pp. 570-575.
69. Huber, D.L. (2005) 'Synthesis, Properties, and Applications of Iron Nanoparticles', *Small*, Vol. 1, pp. 482.
70. Kohler, N., S. Conroy, J. Wang, and M. Zhang (2005) 'Methotrexate-Modified Superparamagnetic Nanoparticles and Their Intracellular Uptake into Human Cancer Cells ', *Langmuir*, Vol. 21, pp. 8858-8864.
71. Desvaux, C., C. Amiens, P. Fejes, P. Renaud, M. Respaud, P. Lecante, E. Snoeck, and B. Chaudret (2005) 'Multimillimetre-large superlattices of air-stable ironÂ–cobalt nanoparticles ', *Nature*, Vol. 4, pp. 750-753.
72. Reiss, G. and A. Hutten (2005) 'Magnetic nanoparticles: Applications beyond data storage ', *Nature Mat.*, Vol. 4, pp. 725-726.

73. Hyeon, T., S.S. Lee, J. Park, Y. Chung, and N.H. B. (2001) 'Synthesis of Highly Crystalline and Monodisperse Maghemite Nanocrystallites without a Size-Selection Process ', *J. Am. Chem. Soc.*, Vol. 123, pp. 12798.
74. Sun, S., H. Zeng, D.B. Robinson, S. Raoux, P.M. Rice, S.X. Wang, and G. Li (2004) 'Monodisperse MFe2O4 (M = Fe, Co, Mn) Nanoparticles ', *J. Am. Chem. Soc.*, Vol. 126, pp. 273-279.
75. Woo, K., J. Hong, S. Choi, H.-W. Lee, J.-P. Ahn, C.S. Kim, and S.W. Lee (2004) 'Easy Synthesis and Magnetic Properties of Iron Oxide Nanoparticles ', *Chem. Mater.*, Vol. 16, pp. 2814-2818.
76. Yang, T., C. Shen, Z. Li, H. Zhang, C. Xiao, S. Chen, Z. Xu, D. Shi, J. Li, and H. Gao (2005) 'Highly Ordered Self-Assembly with Large Area of Fe3O4 Nanoparticles and the Magnetic Properties ', *J. Phys. Chem. B*, Vol. 109, pp. 23233-23236.
77. Jana, N.R., Y. Chen, and X. Peng (2004) 'Size- and Shape-Controlled Magnetic (Cr, Mn, Fe, Co, Ni) Oxide Nanocrystals via a Simple and General Approach ', *Chem. Mater.*, Vol. 16, pp. 3931-3935.
78. Li, Z., Q. Sun, and M.Y. Gao (2005) 'Preparation of Water-Soluble Magnetite Nanocrystals from Hydrated Ferric Salts in 2-Pyrrolidone: Mechanism Leading to Fe3O4', *Angew. Chem. Ind. Ed.*, Vol. 44, pp. 123-126.
79. Li, Z., L. Wei, M.Y. Gao, and H. Lei (2005) 'One-Pot Reaction to Synthesize Biocompatible Magnetite Nanoparticles', *Adv. Mater.*, Vol. 17, pp. 1001-1005.
80. Hu, F.Q., L. Wei, Z. Zhou, Y.L. Ran, Z. Li, and M.Y. Gao (2006) 'Preparation of Biocompatible Magnetite Nanocrystals for In Vivo Magnetic Resonance Detection of Cancer', *Adv. Mater.*, Vol. 18, pp. 2553.
81. Wang, Y., J.F. Wong, X. Teng, X.Z. Lin, and H. Yang (2003) '"Pulling" Nanoparticles into Water: Phase Transfer of Oleic Acid Stabilized Monodisperse Nanoparticles into Aqueous Solutions of -Cyclodextrin ', *Nano Lett.*, Vol. 3, pp. 1555-1559.
82. Euliss, L.E., S.G. Grancharov, S. O'BRIEN, T.J. Deming, G.D. Stucky, C.B. Murray, and G.A. Held (2003) 'Cooperative Assembly of Magnetic Nanoparticles and Block Copolypeptides in Aqueous Media ', *Nano Lett.*, Vol. 3, pp. 1489.
83. Xie, J., C. Xu, Z. Xu, Y. Hou, K.L. Young, S.X. Wang, N. Pourmond, and S. Sun (2006) 'Linking Hydrophilic Macromolecules to Monodisperse Magnetite (Fe3O4) Nanoparticles via Trichloro-s-triazine ', *Chem. Mater.*, Vol. 18, pp. 5401-5403.
84. Li, G., J. Fan, R. Jiang, and Y. Gao (2004) 'Cross-linking the Linear Polymeric Chains in the ATRP Synthesis of Iron Oxide/Polystyrene Core/Shell Nanoparticles ', *Chem. Mater.*, Vol. 16, pp. 1835-1837.
85. Wang, L.Y., J. Luo, Q. Fan, M. Suzuki, I.S. Suzuki, M.H. Englehard, Y.H. Lin, N. Kim, J.Q. Wang, and C.J. Zhong (2005) 'Monodispersed Core-Shell Fe3O4@Au Nanoparticles ', *J. Phys. Chem.*, Vol. 109, pp. 21593-21601.
86. Ban, Z.H., Y.A. Barnakov, F. Li, V.O. Bolub, and C.J. O'Connor (2005) 'The synthesis of core–shell iron@gold nanoparticles and their characterization', *J. Mater. Chem.*, Vol. 15, pp. 4660.
87. Zhang, J., M. Post, T. Veres, Z.J. Jakubek, J. Guan, D. Wang, F. Normandin, Y. Deslandes, and B. Simard (2006) 'Laser-Assisted Synthesis of Superparamagnetic Fe@Au Core-Shell Nanoparticles ', *Phys. Chem. B*, Vol. 110, pp. 7122-7128.
88. Cho, S.-J., J.-C. Idrobo, J. Olamit, K. Liu, N.D. Browning, and S.M. Kauzlarich (2005) 'Growth Mechanisms and Oxidation Resistance of Gold-Coated Iron Nanoparticles ', *Chem. Mater.*, Vol. 17, pp. 3181.
89. Tang, D., R. Yuan, and Y. Chai (2006) 'Magnetic Core-Shell Fe3O4@Ag Nanoparticles Coated Carbon Paste Interface for Studies of Carcinoembryonic Antigen in Clinical Immunoassay ', *J. Phys. Chem. B*, Vol. 110, pp. 11640-11646.
90. Yi, D.K., S.S. Lee, G.C. Papaefthymiou, and J.Y. Ying (2006) 'Nanoparticle Architectures Templated by SiO2/Fe2O3 Nanocomposites ', *Chem. Mater.*, Vol. 18, pp. 614-619.
91. Santra, S., R. Tapec, N. Theodoropoulou, J. Dobson, A. Hebard, and W. Tan (2001) 'Synthesis and Characterization of Silica-Coated Iron Oxide Nanoparticles in Microemulsion: The Effect of Nonionic Surfactants ', *Langmuir*, Vol. 7, pp. 2900-2906.

92. Lu, Y., Y. Yin, B.T. Mayers, and Y. Xia (2002) 'Modifying the Surface Properties of Superparamagnetic Iron Oxide Nanoparticles through A Sol-Gel Approach ', *Nano Lett.*, Vol. 2, pp. 183-186.

93. Zhao, W., J. Gu, L. Zhang, H. Chen, and J. Shi (2005) 'Fabrication of Uniform Magnetic Nanocomposite Spheres with a Magnetic Core/Mesoporous Silica Shell Structure ', *J. Am. Chem. Soc.*, Vol. 127, pp. 8916-8917.

94. Santra, S., R.P. Bagwe, D. Dutta, J.T. Stanley, G.A. Walter, W. Tan, B.M. Moudgil, and R.A. Mericle (2005) 'Synthesis and Characterization of Fluorescent, Radio-Opaque, and Paramagnetic Silica Nanoparticles for Multimodal Bioimaging Applications', *Adv. Mater.*, Vol. 17, pp. 2165-2169.

95. Sun, Y., L. Duan, Z. Guo, Y.D. Mu, M. Ma, L. Xu, Y. Zhang, and N. Gu (2005) 'An improved way to prepare superparamagnetic magnetite-silica core-shell nanoparticles for possible biological application ', *J. Magn. Magn. Mater.*, Vol. 285, pp. 65-70.

96. Salgueiriño-Maceira, V., M.A. Correa-Duarte, M. Farle, A. López-Quintela, K. Sieradzki, and R. Diaz (2006) 'Bifunctional Gold-Coated Magnetic Silica Spheres ', *Chem. Mater.*, Vol. 18, pp. 2701-2706.

97. Salgueiriño-Maceira, V., M.A. Correa-Duarte, M. Spasova, L.M. Liz-Marzán, and M. Farle (2006) 'Composite Silica Spheres with Magnetic and Luminescent Functionalities', *Adv. Func. Mat.*, Vol. 16, pp. 509-514.

98. Vestal, C.R. and Z.J. Zhang (2003) 'Synthesis and Magnetic Characterization of Mn and Co Spinel Ferrite-Silica Nanoparticles with Tunable Magnetic Core ', *Nano Lett.*, Vol. 3, pp. 1739-1743.

99. Ma, D., T. Veres, L. Clime, F. Normandin, J. Guan, D. Kinston, and B. Simard (2007) 'Superparamagnetic FexOy@SiO2 core-shell nanostructure: controlled synthesis and magnetic characterization', *J. Phys. Chem. C (in press)*

100. Tanase, M., L.A. Bauer, A. Hultgren, D.M. Silevitch, L. Sun, D.H. Reich, P.C. Searson, and G.J. Meyer (2001) 'Magnetic alignement of fluorescent nanowires', *Nano Lett.*, Vol. 1, pp. 155-158.

101. Tanase, M., D.M. Silevitch, A. Hultgren, L.A. Bauer, P.C. Searson, G.J. Meter, and D.H. Reich (2002) 'Magnetic trapping and self-assembly of multicomponent nanowires', *J. Appl. Phys.*, Vol: 91, pp. 8549-8551.

102. Tok, J.B.-H., F.Y.S. Chuang, M.C. Kao, K.A. Rose, S.S. Pannu, M.Y. Sha, G. Chakarova, S.G. Penn, and G.M. Dougherty (2006) 'Metallic Striped Nanowires as Multiplexed Immunoassay Platforms for Pathogen Detection', *Angew. Chem. Int. Ed.*, Vol. 45, pp. 6900-6904.

103. Love, J.C., A.R. Urbach, M.G. Prentiss, and G.M. Withesides (2003) 'Three-Dimensional Self-Assembly of Metallic Rods with Submicron Diameters Using Magnetic Interactions ', *J. Am. Chem. Soc.*, Vol. 125, pp. 12696-12697.

104. Piraux, L., S. Dubois, and J.L. Duvail (1999) 'Fabrication and properties of organic and metal nanocylinders in nanoporous membranes ', *J. Mater. Res.*, Vol. 14, pp. 3042-3050.

105. Tsuya, N., T. Tokushima, M. Shiraki, Y. Wakui, Y. Saito, H. Kanamura, S. Hanayo, A. Furugori, and H. Tanaka (1986) 'Alumite disc using anordic oxidation', *IEEE Trans. Magn.*, Vol. 22, pp. 1140-1145.

106. Ciureanu, M., F. Beron, L. Clime, P. Ciureanu, A. Yelon, T.-A. Ovari, R.W. Cochrane, F. Normandin, and T. Veres (2005) 'Magnetic properties of electrodeposited CoFeB thin films and nanowire arrays ', *Electrochim. Acta*, Vol. 50, pp. 4487.

107. Metzger, R.M., V.V. Konovalov, M. Sun, T. Xu, G. Zangari, B. Xu, M. Benkali, and W.D. Doyle (2000) 'Magnetic nanowires in hexagonally ordered pores of alumina', *IEEE Trans. Magn.*, Vol. 36, pp. 30-35.

108. Hurst, S.J., E.K. Payne, L. Qin, and C.A. Mirkin (2006) 'Multisegmented One-Dimensional Nanorods Prepared by Hard-Template Synthetic Methods', *Angew. Chem. Int. Ed.*, Vol. 45, pp. 2672-2692.

109. Dadvand, N., R. Menini, F. Normandin, and T. Veres (2004) *Deposition of nanoelectrocomposite coatings using bath ultrasonic agitation.* in *205-th Meeting of the Electrochemical Society*. San Antonio, TX, USA.

110. Duvail, J.L., S. Dubois, L. Piraux, A. Vaures, A. Fert, D. Adam, M. Champagne, F. Rousseaux, and D. Decanini (1998) 'Electrodeposition of patterned magnetic nanostructures', *J. Appl. Phys.*, Vol. 84, pp. 6359-6365.

111. Masuda, H. and A. Fukuda (1995) 'Ordered Metal Nanohole Arrays Made by a Two-Step Replication of Honeycomb Structures of Anodic Alumina ', *Science*, Vol. 268, pp. 1466-1468.

112. Xu, T.T., R.D. Piner, and R.S. Ruoff (2003) 'An Improved Method To Strip Aluminum from Porous Anodic Alumina Films ', *Langmuir*, Vol. 19, pp. 1443-1445.

113. Li, L., G. Li, Y. Zhang, Y. Yang, and L. Zhang (2004) 'Pulsed Electrodeposition of Large-Area, Ordered Bi1-xSbx Nanowire Arrays from Aqueous Solutions ', *J. Phys. Chem. B.*, Vol. 108, pp. 19380.

114. Mardilovich, P.P., A.N. Govyadinov, N.I. Mukhurov, A.M. Rzhevskii, and R. Paterson (1995) 'New and modified anodic alumina membranes Part I. Thermotreatment of anodic alumina membranes ', *J. Membr. Sci.*, Vol. 98, pp. 131

115. de L. Lira, H. and R. Paterson (2002) 'New and modified anodic alumina membranes. Part III. Preparation and characterisation by gas diffusion of 5 nm pore size anodic alumina membranes', *J. Membr. Sci.*, Vol. 206, pp. 375-378.

116. Yuan, J.H., F.Y. He, D.C. Sun, and X.H. Xia (2004) 'A Simple Method for Preparation of Through-Hole Porous Anodic Alumina Membrane ', *Chem. Mater.*, Vol. 16, pp. 1841-1844.

117. Barbic, M. (2002) 'Magnetic wires in MEMS and bio-medical applications', *J. Magn. Magn. Mater.*, Vol. 249, pp. 357-367.

118. Reich, D.H., M. Tanase, A. Hultgren, L.A. Bauer, C.S. Chen, and G.J. Meyer (2003) 'Biological applications of multifunctional magnetic nanowires', *J. Appl. Phys.*, Vol. 93, pp. 7275-7280.

119. Brown Jr., W.F. (1966) *Magnetostatic principles in ferromagnetism*. Springer, New York.

120. Fredkin, D.R. and T.R. Koehler (1987) 'Numerical micromagnetics by the finite element method', *IEEE Trans. Magn.*, Vol. MAG-23, pp. 3385-3387.

121. Koehler, T.R. and D.R. Fredkin (1992) 'Finite element methods for micromagnetics', *IEEE Trans. Magn.*, Vol. 28, pp. 1239.

122. Greengard, L. and V. Rokhlin (1987) 'A fast algorithm for particle simulations', *J. Comp. Phys.*, Vol. 73, pp. 325-348.

123. Donahue, M.J. and D.G. Porter, *OOMMF User's guide, version 1.0*. 1999, National Institute of Standards and Technology: Gaithesburg, MD.

124. Scholz, W., D. Suess, R. Dittrich, T. Schrefl, V. Tsiantos, H. Forster, and J. Fidler (2004) 'Implementation of high performance parallel finite element micromagnetics', *J. Magn. Magn. Mater.*, Vol. 272-276, pp. 693-694.

125. Kruzic, M. and A. Prohl (2006) 'Recent developments in the modeling, analysis, and numerics of ferromagnetism', *SIAM*, Vol. 48, pp. 439-483.

126. Bagster, D.F. (1987) 'The calculation of force on a weakly magnetic particle in a magnetic field', *Int. J. Min. Process.*, Vol. 20, pp. 1-15.

127. Clime, L., P. Ciureanu, and A. Yelon (2006) 'Magnetostatic interactions in dense nanowire arrays', *J. Magn. Magn. Mater.*, Vol. 297, pp. 60.

128. Tejada, J., X.X. Zhang, and J.M. Hernandez (1997) *Proceedings of Magnetic Hysteresis in Novel Magnetic Materials: Proceedings of the NATO Advanced Study Institute, Mykonos, Greece, 1-12 July 1996*. NATO Science Series: E, ed. H. Hadjipanayis. Kluwer Academic Publishers, Norwell, MA.

129. Luo, W., S.R. Nagel, T.F. Rosenbaum, and R.E. Rosensweig (1991) 'Dipole interactions with random anisotropy in a frozed ferrofluid', *Phys. Rev. Lett.*, Vol. 67, pp. 2721-2724.

130. Tejada, J., X.X. Zhang, E. del Barco, J.M. Hernández, and E.M. Chudnovsky (1997) 'Macroscopic Resonant Tunneling of Magnetization in Ferritin', *Phys. Rev. Lett.*, Vol. 79, pp. 1754-1757.

131. Friedman, J.R., U. Voskoboynik, and M.P. Sarachik (1997) 'Anomalous magnetic relaxation in ferritin', *Phys. Rev. B*, Vol. 56, pp. 10793-10796.

132. Gider, S., D.D. Awschalom, T. Douglas, K. Wong, S. Mann, and G. Cain (1996) 'Classical and quantum magnetism in synthetic ferritin proteins', *J. Appl. Phys.*, Vol. 79, pp. 5324-5326.

133. Sappey, R., E. Vincent, N. Hadacek, F. Chaput, J.P. Boilot, and D. Zins (1997) 'Nonmonotonic field dependence of zero-field cooled magnetization peak in some systems of magnetic nanoparticles', *Phys. Rev. B*, Vol. 56, pp. 14551.
134. Wang, L., J. Ding, H.Z. Kong, Y. Li, and Y.P. Feng (2001) 'Monte Carlo simulation of a cluster system with strong interaction and random anisotropy', *Phys. Rev. B*, Vol. 64, pp. 214410.
135. Dimitrov, D.A. and G.M. Wysin (1996) 'Magnetic properties of superparamagnetic particles by a Monte Carlo method', *Phys. Rev. B*, Vol. 54, pp. 9237-9241.
136. Stancu, A. and L. Spinu (1998) 'Temperature- and time-dependent Preisach model for a Stoner-Wohlfarth particle system', *IEEE Trans. Magn.*, Vol. 34, pp. 3867-3875.
137. Gubin, S.P. and Y.A. Koksharov (2002) 'Preparation, structure, and properties of magnetic materials based on Co-containing nanoparticles', *Inorg. Mat.*, Vol. 38, pp. 1085-1099.
138. Andersson, J.-O., C. Djurberg, T. Jonsson, P. Svendlindh, and P. Nordblad (1997) 'Monte Carlo studies of the dynamics of an interacting monodispersive magnetic-particle system', *Phys. Rev. B*, Vol. 56, pp. 13983-13988.
139. Stoner, E.C. and E.P. Wohlfarth (1991) 'A mechanism of magnetic hysteresis in heterogeneous alloys', *IEEE Trans. Magn.*, Vol. 27, pp. 3475.
140. Wohlfarth, E.P. (1979) 'The temperature dependence of the magnetic susceptibility of spin glasses', *Phys. Lett.*, Vol. 70A, pp. 489-491.
141. Allia, P., M. Ciosson, P. Tiberto, F. Vinai, M. Knobel, M.A. Novak, and W.C. Nunes (2001) 'Granular Cu-Co alloys as interacting superparamagnets', *Phys. Rev. B*, Vol. 64, pp. 144420.
142. Poddar, P., T. Telem-Shafir, T. Fried, and G. Magkovich (2002) 'Dipolar interactions in two- and three-dimensional nanoparticle arrays', *Phys. Rev. B*, Vol. 66, pp. 060403(R).
143. Bertorello, H.R., M.I. Oliva, and P.G. Bercoff (2004) 'Energy barriers for magnetization reversal of partial exchange-coupled particles', *J. Alloy. Comp.*, Vol. 369, pp. 62-65.
144. Mayergoyz, I.D. (1986) 'Mathematical models of hysteresis', *Phys. Rev. Lett.*, Vol. 56, pp. 1518-1521.
145. Mayergoyz, I.D. (1991) *Mathematical models of hysteresis*. Springer-Verlag, New York.
146. Preisach, F. (1935) 'Über die magnetische Nachwirkung', *Z. Phys.*, Vol. 94, pp. 277-302.
147. Muxworthy, A.R., D. Heslop, and W. Williams (2004) 'Influence of magnetostatic interactions on first-order-reversal-curve (FORC) diagrams: a micromagnetic approach', *Geophys. J. Int.*, Vol. 158, pp. 888.
148. Pike, C.R., A.P. Roberts, and K.L. Verosub (1999) 'Characterizing interactions in fine magnetic particle systems using first order reversal curves', *J. Appl. Phys.*, Vol. 85, pp. 6660.
149. Pike, C. and A. Fernandez (1999) 'An investigation of magnetic reversal in submicron-scale Co dots using first order reversal curve diagrams', *J. Appl. Phys.*, Vol. 85, pp. 6668.
150. Pike, C.R. (2003) 'First-order reversal-curve diagrams and reversible magnetization', *Phys. Rev. B*, Vol. 68, pp. 104424.
151. Roberts, A.P., C.R. Pike, and K.L. Verosub (2000) 'First-order reversal curve diagrams: a new tool for characterizing the magnetic properties of natural samples', *J. Geophys. Res.*, Vol. 105, pp. 28,461.
152. Spinu, L., A. Stancu, C. Radu, F. Li, and J.B. Wiley (2004) 'Method of magnetic characterization of nanowire structures', *IEEE Trans. Magn.*, Vol. 40, pp. 2116.
153. Néel, L. (1954) 'Remarques sur la théorie des propriétés magnétiques des substances dures', *Appl. Sci. Res.*, Vol. 4, pp. 13-24.
154. Winklhofer, M. and G.T. Zimanyi (2006) 'Extracting the intrinsic switching field distributionin perpendicular media: a comparative analysis', *J. Appl. Phys.*, Vol. 99, pp. 08E710-3.
155. Carvallo, C., A.R. Muxworthy, D.J. Dunlop, and W. Williams (2003) 'Micromagnetic modeling of first-order reversal curve (FORC) diagrams for single-domain and pseudo-single-domain magnetite', *Earth Planet. Sci. Lett.*, Vol. 213, pp. 375.
156. Stancu, A., C. Pike, L. Stoleriu, P. Postolache, and D. Cimpoesu (2003) 'Micromagnetic and Preisach analysis of First Order Reversal Curves (FORC) diagram', *J. Appl. Phys.*, Vol. 93, pp. 6620.

157. Carvallo, C., D.J. Dunlop, and O. Ozdemir (2005) 'Experimental comparison of FORC and remanent Preisach diagrams', *Geophys. J. Int.*, Vol. 162, pp. 747.
158. Stancu, A. and P. Andrei (2006) 'Characterization of static hysteresis models using first-order reversal curves diagram method', *Physica B*, Vol. 372, pp. 72-75.
159. Spinu, L., A. Stancu, C. Radu, F. Li, and J.B. Wiley (2004) 'Method of magnetic characterization of nanowire structures', *IEEE Trans. Magn.*, Vol. 40, pp. 2116-2118.
160. Natali, M., I.L. Prejbeanu, A. Lelib, L.D. Buda, K. Ounadjela, and Y. Chen (2002) 'Correlated magnetic vortex chains in mesoscopic cobalt dot arrays', *Phys. Rev. Lett.*, Vol. 88, pp. 157203-1.
161. Pulwey, R., M. Rahm, J. Biberger, and D. Weiss (2001) 'Switching behavior of vortex structures in nanodisks', *IEEE Trans. Magn.*, Vol. 37, pp. 2076.
162. Shinjo, T., T. Okuno, R. Hassdorf, K. Shigeto, and T. Ono (2001) 'Magnetic vortex core observation in circular dots of permalloy', *Science*, Vol. 289, pp. 5481.
163. Schneider, M., H. Hoffmann, and J. Zweck (2000) 'Lorentz microscopy of circular ferromagnetic permalloy nanodisks', *Appl. Phys. Lett.*, Vol. 77, pp. 2909.
164. Cowburn, R.P., D.K. Koltsov, A.O. Adeyeye, M.E. Welland, and D.M. Tricker (1999) 'Single-domain circular nanomagnets', *Phys. Rev. Lett.*, Vol. 83, pp. 1042.
165. Slovakova, M., N. Minc, Z. Bilkova, C. Smajda, W. Faigle, C. Futterer, M. Taverna, and J.-L. Viovy (2005) 'Use of self assembled magnetic beads for on-chip protein digestion', *Lab Chip*, Vol. 5, pp. 935-942.
166. Deng, T., M. Prentiss, and G.M. Withesides (2001) 'Fabrication and magnetic microfiltration system using soft lithography', *Appl. Phys. Lett.*, Vol. 80, pp. 461-463.
167. Mirowski, E., J. Moreland, S. Russek, and M.J. Donahue (2004) 'Integrated microfluidic isolation platform for magnetic particle manipulation in biological systems', *Appl. Phys. Lett.*, Vol. 84, pp. 1786-1788.
168. Dubus, S., J.-F. Gravel, B. Le Drogoff, P. Nobert, T. Veres, and D. Boudreau (2006) 'PCR-free DNA detection using a magnetic bead-supported polymeric transducer and microelectromagnetic traps', *Anal. Chem.*, Vol. 78, pp. 4457-4464.
169. Deng, T., G.M. Withesides, M. Radhakrishnan, G. Zabow, and M. Prentiss (2001) 'Manipulation of magnetic microbeads in suspension using micromagnetic system fabricated with soft lithography', *Appl. Phys. Lett.*, Vol. 78, pp. 1775-1777.
170. Choi, J.-W., C.H. Ahn, S. Bhansali, and H. Thurman Henderson (2000) 'A new magnetic bead-based bio-separator with planar electromagnet surfaces for integrated bio-detection systems', *Sens. Act. B*, Vol. 68, pp. 34-39.
171. Choi, J.-W., T.M. Liakopoulos, and C.H. Ahn (2001) 'An on-chip magnetic bead separator using spiral electromagnets with semi-encapsulated permalloy', *Biosens. Bioel.*, Vol. 16, pp. 409-416.
172. Ademtech,www.ademtech.com
173. Invitrogen,www.invitrogen.com/dynal
174. Mattews, M.T. and J.M. Hill (2006) 'Flow around nanospheres and nanocylinders', *Q. Jl Mech. Appl. Math.*, Vol. 59, pp. 191-210.